atoms

MDPI

Article

Pseudo-Relativistic Hartree–Fock and Fully Relativistic Dirac–Hartree–Fock Calculations of Radiative Parameters in the Fifth Spectrum of Lutetium (Lu V)

Lucas Maison [1], Helena Carvajal Gallego [1] and Pascal Quinet [1,2,*]

[1] Physique Atomique et Astrophysique, Université de Mons, B-7000 Mons, Belgium
[2] IPNAS, Université de Liège, B-4000 Liège, Belgium
* Correspondence: pascal.quinet@umons.ac.be; Tel.: +32-65-373629

Abstract: Using two independent theoretical methods based on the pseudo-relativistic Hartree–Fock (HFR) and the fully relativistic Multiconfigurational Dirac–Hartree–Fock (MCDHF) approaches, we computed the radiative parameters (transition probabilities and oscillator strengths) corresponding to the spectrum of quadruply ionized lutetium (Lu V). The agreement observed between both sets of results allowed us to deduce the radiative rates for a large amount of transitions in order to calculate the contribution of this ion to the opacity of kilonovae in their early phases, i.e., for T = 25,000 K. The results obtained were compared to previous data computed for other quadruply ionized lanthanide atoms, namely La V, Ce V, Pr V, Nd V and Pm V, in order to highlight the main contributors to the opacity among these ions under kilonovae conditions where the V^{th} spectra are predominant.

Keywords: atomic data; lanthanides; oscillator strengths; transition probabilities; opacity; kilonova

check for updates

Citation: Maison, L.; Carvajal Gallego, H.; Quinet, P. Pseudo-Relativistic Hartree–Fock and Fully Relativistic Dirac–Hartree–Fock Calculations of Radiative Parameters in the Fifth Spectrum of Lutetium (Lu V). *Atoms* **2022**, *10*, 130. https://doi.org/10.3390/atoms10040130

Academic Editor: Christian Parigger

Received: 29 August 2022
Accepted: 21 October 2022
Published: 2 November 2022

1. Introduction

Quadruply ionized lutetium (Lu V) belongs to the holmium isoelectronic sequence. Because of the collapse of the 4f orbital, its ground configuration is not the same as other Ho-like elements. Indeed, according to the NIST database [1], the fundamental configuration of Lu V is $5p^64f^{13}$, while it is $5p^64f^{11}6s^2$ and $5p^64f^{12}6s$ for the first two members of the sequence, Ho I and Er II, respectively, and $5p^54f^{14}$ for higher ionization stages along the sequence, from Re IX. This makes systematic experimental and theoretical isoelectronic studies quite complicated and explains why these spectra are poorly or not at all known. The behavior of the 4f orbital for the ground configurations along the holmium isoelectronic sequence is shown in Figure 1.

The first (and most complete) experimental analysis of the Lu V spectrum dates back to 1978 with the paper by Kaufman and Sugar [2] in which 419 lines were classified as transitions among 136 energy levels belonging to the $4f^{13}$, $4f^{12}5d$, $4f^{12}6s$ and $4f^{12}6p$ configurations on the basis of observations made from a sliding spark discharge using a 10.7 m normal incidence spectrograph in the range of 500–2100 Å. Calculated energy levels and eigenvectors, obtained with a limited configuration interaction model utilizing the Racah algebra techniques [3] and a semi-empirical adjustment of radial integrals, were also reported in this paper. More recently, parametric calculations in Lu V were performed by Ryabtsev et al. [4] with the pseudo-relativistic Hartree–Fock (HFR) method implemented in the Cowan codes [5]. By comparing their calculated transition probabilities with the line intensities taken from an unpublished list of wavelengths initially considered (but not classified) as Lu V by Kaufman and Sugar [6], Ryabtsev et al. were able to identify seven new levels using 20 experimental lines from 563 to 978 Å. It should be noted that the latter authors also gave the calculated transition probabilities only for these 20 transitions, with no radiative rate having been published to date for the few hundred other lines experimentally measured in Lu V.

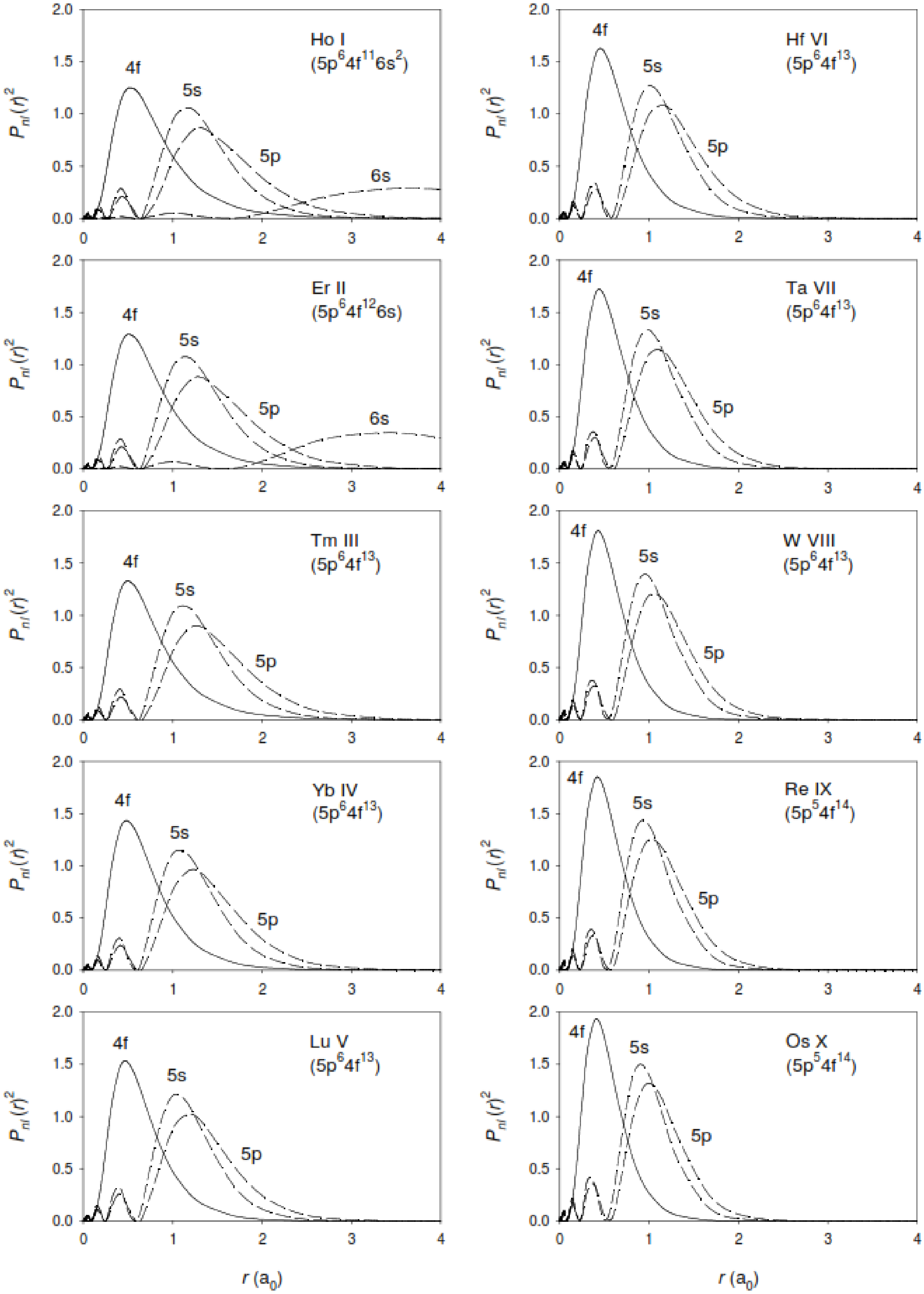

Figure 1. Electron probability densities ($P_{nl}(r)^2$) of the outermost orbitals in the ground configurations along the holmium isoelectronic sequence, from Ho I to Os X.

The main goal of the present work is to fill this gap and to provide a consistent set of transition probabilities and oscillator strengths for all lines identified in the Lu V spectrum. For this purpose, two independent theoretical methods were used, namely the pseudo-relativistic Hartree–Fock (HFR) and the purely relativistic Multiconfigurational Dirac–Hartree–Fock (MCDHF) approaches, by considering configuration interactions as completely as possible in each of these methods. This is the only way to estimate the quality of the results obtained through the detailed and systematic comparison of the calculated radiative parameters, in the absence of other available experimental or theoretical data.

It is important to recall here that the radiative parameters characterizing the lanthanide ions, such as Lu V, are of great interest for the analysis of laboratory and astrophysical plasmas. More particularly, the ejected material from neutron star mergers, called kilonova, such as the one observed just after the famous detection of gravitational waves on 17 August 2017 (also known as the GW170817 event) [7], provided the first evidence for the astrophysical site of synthesis of heavy elements through the rapid neutron capture process or r-process [8]. Among these heavy elements, given the high density and richness of their spectra (often comprising several hundred thousand or even several million lines), the lanthanide ions were found to strongly contribute to the opacity affecting the kilonova spectra [9]. This opacity, which is a key parameter for the determination of the kilonova light curve, i.e., the evolution of light intensity as a function of time, can only be reliably estimated by the knowledge of the most accurate atomic data possible for a sufficient number of spectral lines belonging to the elements of interest, in different ionization stages. Applications to the opacity determination of the new radiative parameters computed in our work for Lu V transitions are also discussed in the present paper, which is part of our systematic investigation of moderately ionized lanthanides already started with recent similar works on atomic and opacity calculations in La V-X [10], Ce V-X [11], Pr V-X, Nd V-X, and Pm V-X [12] ions.

2. Atomic Structure and Radiative Rate Calculations

2.1. Pseudo-Relativistic Hartree–Fock Method

The first method used for modeling the atomic structure and computing the radiative parameters in Lu V was the pseudo-relativistic Hartree–Fock (HFR) approach developed by Cowan [5], using the suite of codes RCN, RCN2 and RCG adapted by the Atomic Physics and Astrophysics group of Mons University for the atomic structure calculations in heavy elements [13]. Configuration interaction was considered by explicitly including in the calculations the $4f^{13}$, $4f^{12}6p$, $4f^{12}7p$, $4f^{12}8p$, $4f^{12}5f$, $4f^{12}6f$, $4f^{12}7f$, $4f^{12}8f$, $4f^{11}5d^2$, $4f^{11}6s^2$, $4f^{11}6p^2$, $4f^{11}5d6s$, $5p^54f^{14}$, $5p^54f^{13}6p$ odd-parity configurations, and the $4f^{12}6s$, $4f^{12}7s$, $4f^{12}8s$, $4f^{12}5d$, $4f^{12}6d$, $4f^{12}7d$, $4f^{12}8d$, $4f^{12}5g$, $4f^{12}6g$, $4f^{12}7g$, $4f^{12}8g$, $4f^{11}6s6p$, $4f^{11}5d6p$, $5p^54f^{13}6s$ and $5p^54f^{13}5d$ even-parity configurations. These configurations represent the majority of those lying (and overlapping) below the Lu V ionization potential, as shown in Figures 2 and 3, where their energy ranges, estimated from Monoconfigurational HFR calculations, are plotted for odd and even parities, respectively. Some additional configurations with open 5s subshell are also reported in these figures in order to show their high energy positions (well above the ionization potential) and thus their weak interaction with lower configurations of interest. It was verified that the inclusion of configurations of the type $5s5p^64f^{14}$, $5s5p^64f^{13}5d$, $5s5p^64f^{13}6s$ and $5s5p^64f^{13}6p$ had a negligible impact on the radiative transitions considered in this work. It is also worth mentioning that, as the list of configurations mentioned above accounts for the main core–valence interactions via electron excitations from the 4f and 5p orbitals, core polarization corrections, such as those developed in the so-called HFR + CPOL method [14,15], were not introduced here. This is confirmed by the negligible role of the configurations involving excitation of the 5s core electrons, as discussed above.

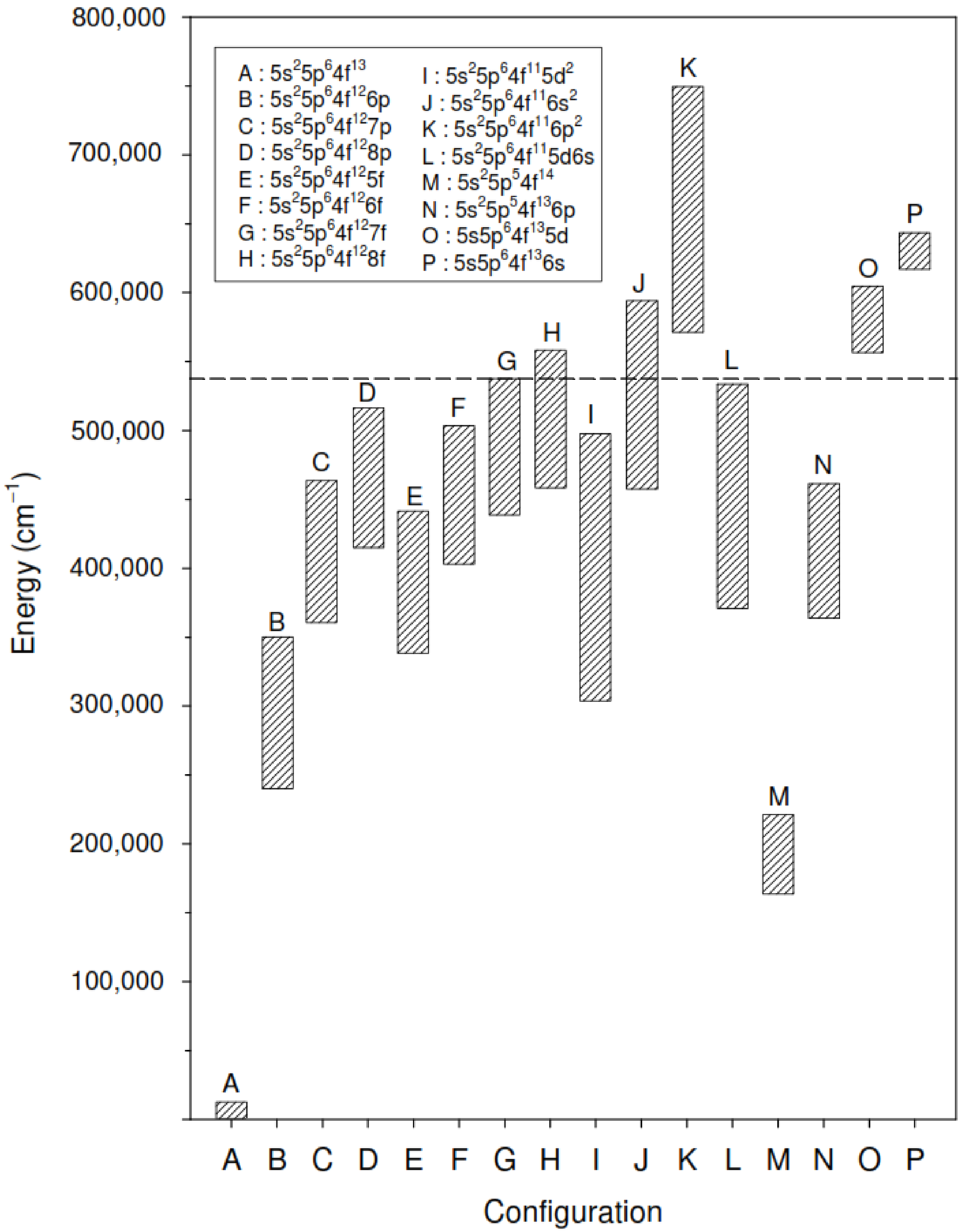

Figure 2. Energy ranges of odd configurations in Lu V predicted by HFR calculations. The dashed line represents the ionization energy taken from the NIST database [1].

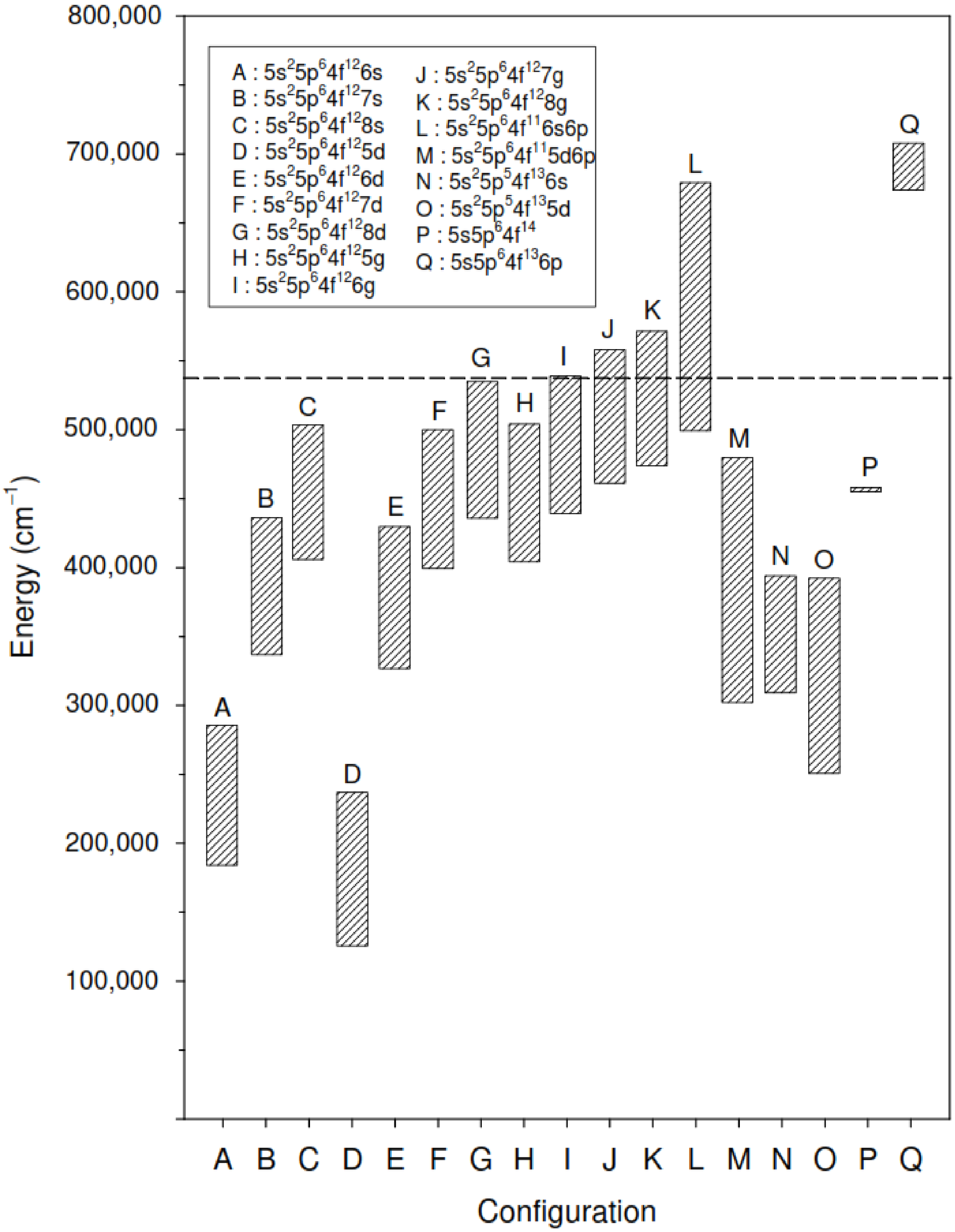

Figure 3. Energy ranges of even configurations in Lu V predicted by HFR calculations. The dashed line represents the ionization energy taken from the NIST database [1].

Unfortunately, the large size of our HFR model did not allow us to consider the well-established semi-empirical fitting procedure of energy levels with the RCE program [5]. Therefore, the average energies (E_{av}) of the $4f^{13}$, $4f^{12}5d$, $4f^{12}6s$ and $4f^{12}6p$ configurations were adjusted in order to reproduce as well as possible the lowest level known experimentally in each of these configurations. In addition, the interactions with distant configurations not introduced in the multi-configuration expansions were considered by scaling down the Slater parameters characterizing the Coulomb electrostatic interactions between electrons within the same configuration (F^k, G^k), and between electrons belonging to different configurations (R^k), as recommended by Cowan [5]. More precisely, for the electrostatic integrals, different scaling factors (*SF*) such as 0.80, 0.85 and 0.90 were used in our calculations, keeping the spin–orbit parameters to their ab initio values. Even if these three *SF*-values proved to be rather similar to reproduce the observed energy spectrum (within a few tenths of a percent), *SF* = 0.85 was found to give the smallest differences between the calculated energy levels and those experimentally measured by Kaufman and Sugar [2] and Ryabtsev et al. [4], the mean relative deviations $\Delta E/E_{\mathrm{exp}}$ (where $\Delta E = E_{\mathrm{calc}} - E_{\mathrm{exp}}$) being equal to -0.0032 ± 0.0030, 0.0005 ± 0.0036 and 0.0044 ± 0.0060 for *SF* = 0.80, 0.85 and 0.90, respectively. This is shown in Figure 4, where $\Delta E/E_{\mathrm{exp}}$ is plotted as a function of E_{exp} for the different scaling factors considered. The HFR model with *SF* = 0.85 was then adopted to determine the radiative parameters in Lu V.

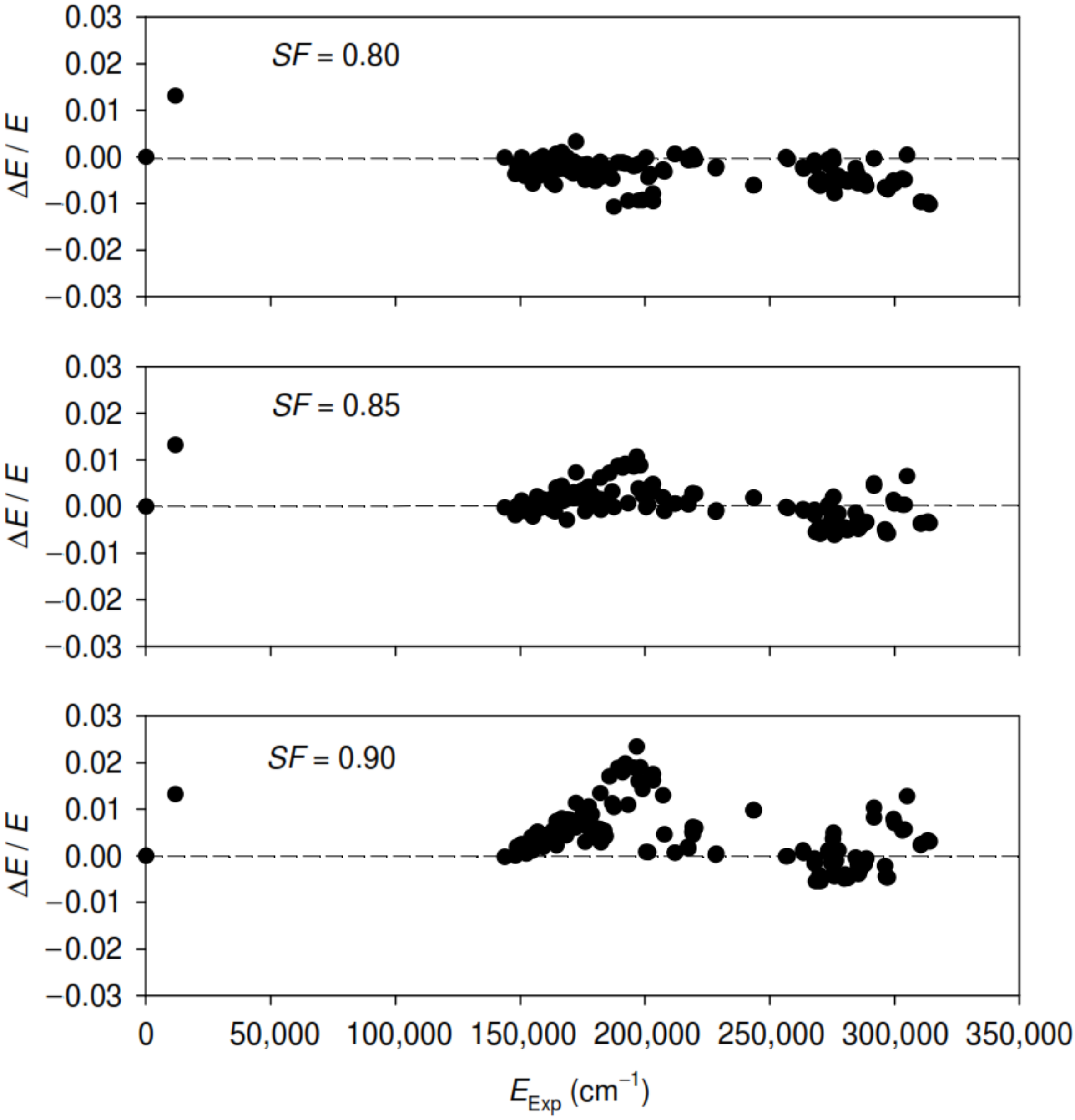

Figure 4. Relative deviations $\Delta E/E$ (with $\Delta E = E_{\mathrm{Calc}} - E_{\mathrm{Exp}}$ and $E = E_{\mathrm{Exp}}$) as a function of known experimental energy levels [2,4] for HFR calculations with scaling factors *SF* = 0.80, 0.85 and 0.90.

2.2. Fully Relativistic Multiconfiguration Dirac–Hartree–Fock Method

The second theoretical method used for the study of atomic properties in Lu V was the Multiconfiguration Dirac–Hartree–Fock (MCDHF) method developed by Grant [16] and Froese Fischer et al. [17] using the latest version of GRASP (General Relativistic Atomic Structure Program), GRASP2018 [18]. High-order relativistic effects, i.e., the Breit interaction, QED self-energy and vacuum polarization corrections, were incorporated in the relativistic configuration interaction step of the GRASP2018 package.

As a starting point, a multi-reference (MR) was defined from the experimentally known configurations, i.e., $4f^{13}$, $4f^{12}5d$, $4f^{12}6s$ and $4f^{12}6p$, where the orbitals from 1s to 4f were optimized on the $4f^{13}$ ground configuration while 5d, 6s and 6p were optimized on the $4f^{12}5d$, $4f^{12}6s$ and $4f^{12}6p$ configurations, with all the other orbitals being frozen. From this MR, different physical models were implemented in order to optimize the wave functions and the corresponding energy levels by gradually increasing the basis of configuration state functions (CSFs), and thus taking into account more correlations. In a first step, different valence–valence (VV) models, in which single and double excitations (SD) of valence electrons, i.e., occupying open subshells of configurations from the MR to a set of active spectroscopic orbitals, were considered in order to generate the CSF expansions. These sets of active orbitals are denoted $\{n\mathrm{s}, n'\mathrm{p}, n''\mathrm{d}, \ldots\}$, where n, n', n'', … are the maximum principal quantum numbers considered for each azimuthal quantum number l. A first VV model (VV1) was built by adding to the MR configurations, SD excitations from 4f, 5d, 6s, 6p to the {6s,6p,5d,5f,5g} active set (J = 1/2–19/2). Only the new orbitals were optimized, the other ones being kept to their values obtained before. The same strategy was used to build the more elaborate VV2 and VV3 models in which the {6s,6p,6d,6f,5g} and {7s,7p,7d,6f,5g} active sets were considered, respectively. These calculations gave rise to 415,613 (VV1), 1,327,923 (VV2) and 2,253,529 (VV3) CSFs when considering both parities together. Finally, from the VV3 model, a core–valence (CV) model was built by adding SD excitations from the 5s and 5p core orbitals to the unfilled subshells involved in the MR configurations, i.e., 4f, 5d, 6s and 6p, leading to calculations including a total of 2,301,648 CSFs (J = 1/2–19/2).

It was verified that the MCDHF energy level values obtained in our different models showed a better agreement with available experimental results [2,4] when going from the simplest approximation (MR) to the most elaborate one (CV), the mean relative deviations $\Delta E/E_{\mathrm{exp}}$ (where $\Delta E = E_{\mathrm{calc}} - E_{\mathrm{exp}}$) being found to be equal to 0.0725 ± 0.0169, 0.0618 ± 0.0152, 0.0306 ± 0.0144, 0.0308 ± 0.0127 and 0.0110 ± 0.0149 when considering the MR, VV1, VV2, VV3 and CV models, respectively. This is illustrated in Figure 5, showing the evolution of the agreement between the computed and the experimental energy levels as a function of the MCDHF model considered.

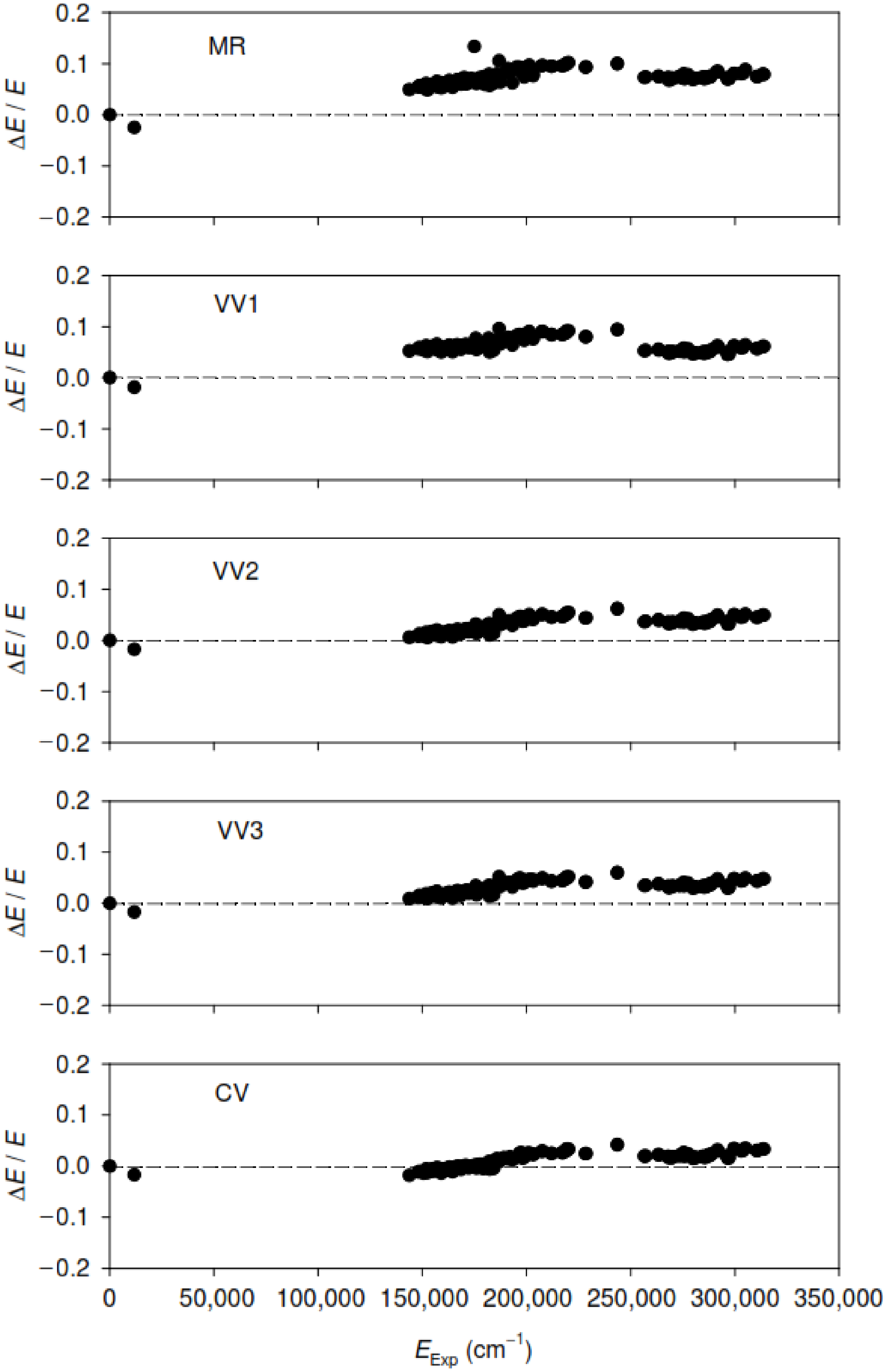

Figure 5. Relative deviations $\Delta E/E$ (with $\Delta E = E_{\mathrm{Calc}} - E_{\mathrm{Exp}}$ and $E = E_{\mathrm{Exp}}$) as a function of known experimental energy levels [2,4] for MCDHF calculations in MR, VV1, VV2, VV3 and CV models.

3. Transition Probabilities and Oscillator Strengths

The transition probabilities (*gA*) and oscillator strengths (log *gf*) computed in the present work using the HFR and MCDHF methods are reported in Table 1 for all the experimentally observed lines of Lu V taken from Kaufman and Sugar [2] and Ryabtsev et al. [4].

Table 1. Calculated transition probabilities (*gA*) and oscillator strengths (log *gf*) for experimentally observed spectral lines in Lu V.

	Lower Level [b]			Upper Level [b]			gA (s^{-1}) [c]		log gf [c]	
λ (Å) [a]	**E (cm^{-1})**	**(P)**	**J**	**E (cm^{-1})**	**(P)**	**J**	**HFR [d]**	**MCDHF [e]**	**HFR [d]**	**MCDHF [e]**
504.825	0	(o)	7/2	198,089	(e)	7/2	2.43×10^{8} *	1.80×10^{8}	−2.04 *	−2.18
508.374	0	(o)	7/2	196,706	(e)	5/2	2.96×10^{8} *	7.75×10^{8}	−1.95 *	−1.54
511.664	0	(o)	7/2	195,441	(e)	5/2	1.43×10^{9}	1.43×10^{9}	−1.26	−1.27
520.559	0	(o)	7/2	192,100	(e)	9/2	5.63×10^{7} *	4.56×10^{7} #	−2.65 *	−2.75 #
523.569	0	(o)	7/2	190,994	(e)	5/2	1.25×10^{9}	1.51×10^{9}	−1.30	−1.22
528.571	0	(o)	7/2	189,188	(e)	7/2	8.00×10^{7} *	1.18×10^{8} #	−2.48 *	−2.32 #
535.277	0	(o)	7/2	186,818	(e)	5/2	1.51×10^{9}	1.38×10^{9}	−1.19	−1.23
536.778	11,793	(o)	5/2	198,089	(e)	7/2	5.22×10^{7} *	4.53×10^{7} #	−2.65 *	−2.72 #
538.398	0	(o)	7/2	185,736	(e)	7/2	3.99×10^{7} *	1.09×10^{6} #	−2.77 *	−4.34 #
540.794	11,793	(o)	5/2	196,706	(e)	5/2	1.19×10^{8} *	1.59×10^{5} #	−2.29 *	−5.18 #
544.518	0	(o)	7/2	183,649	(e)	9/2	9.56×10^{8}	6.61×10^{8} #	−1.37	−1.53 #
	11,793	(o)	5/2	195,441	(e)	5/2	1.91×10^{9}	1.54×10^{9}	−1.08	−1.18
549.375	0	(o)	7/2	182,025	(e)	5/2	1.93×10^{8} *	2.08×10^{7}	−2.06 *	−3.03
549.772	0	(o)	7/2	181,894	(e)	7/2	5.14×10^{8} *	6.97×10^{8}	−1.63 *	−1.50
555.444	0	(o)	7/2	180,036	(e)	7/2	2.69×10^{9}	4.00×10^{9}	−0.91	−0.73
558.024	0	(o)	7/2	179,203	(e)	5/2	3.15×10^{7} *	2.58×10^{9}	−2.83 *	−0.92
	11,793	(o)	5/2	190,994	(e)	5/2	2.57×10^{8} *	1.12×10^{8}	−1.93 *	−2.30
563.723	0	(o)	7/2	177,396	(e)	9/2	3.88×10^{8}	3.17×10^{8} #	−1.73	−1.82 #
	0	(o)	7/2	177,390	(e)	5/2	2.93×10^{9}	3.39×10^{8}	−0.86	−1.80
	11,793	(o)	5/2	189,188	(e)	7/2	5.53×10^{6} *	1.39×10^{7} #	−3.58 *	−3.19 #
569.300	0	(o)	7/2	175,654	(e)	7/2	1.59×10^{9}	1.95×10^{9}	−1.11	−1.03
571.346	11,793	(o)	5/2	186,818	(e)	5/2	7.06×10^{9}	6.40×10^{9}	−0.46	−0.51
574.902	11,793	(o)	5/2	185,736	(e)	7/2	1.19×10^{8} *	7.90×10^{7} #	−2.23 *	−2.42 #
576.300	0	(o)	7/2	173,520	(e)	7/2	2.17×10^{9}	1.18×10^{9}	−0.97	−1.23
580.580	0	(o)	9/2	172,242	(e)	9/2	4.23×10^{8}	4.08×10^{8}	−1.67	−1.68
583.746	0	(o)	7/2	171,307	(e)	7/2	1.67×10^{9}	1.22×10^{9}	−1.07	−1.21
584.778	0	(o)	7/2	171,005	(e)	5/2	1.68×10^{8} *	3.81×10^{8}	−2.07 *	−1.71
587.432	11,793	(o)	5/2	182,025	(e)	5/2	9.16×10^{8}	1.46×10^{9}	−1.33	−1.13
587.887	11,793	(o)	5/2	181,894	(e)	7/2	8.62×10^{5} *	9.55×10^{6} #	−4.35 *	−3.30 #
588.156	0	(o)	7/2	170,023	(e)	5/2	5.66×10^{8} *	1.30×10^{8}	−1.53 *	−2.17
594.380	11,793	(o)	5/2	180,036	(e)	7/2	2.04×10^{9}	1.68×10^{9}	−0.97	−1.05
597.338	11,793	(o)	5/2	179,203	(e)	5/2	7.72×10^{8}	3.85×10^{7} #	−1.38	−2.68 #
598.004	0	(o)	7/2	167,223	(e)	5/2	1.33×10^{8} *	5.25×10^{6}	−2.15 *	−3.55
600.328	0	(o)	7/2	166,577	(e)	5/2	1.63×10^{8}	2.56×10^{8}	−2.06	−1.86
600.470	0	(o)	7/2	166,535	(e)	7/2	1.02×10^{8} *	1.18×10^{8}	−2.26 *	−2.19
601.537	0	(o)	7/2	166,240	(e)	9/2	1.44×10^{9}	9.59×10^{8}	−1.11	−1.28
609.013	0	(o)	7/2	164,198	(e)	7/2	1.06×10^{8} *	1.69×10^{5} #	−2.23 *	−5.02 #
610.275	11,793	(o)	5/2	175,654	(e)	7/2	7.69×10^{7} *	1.58×10^{8}	−2.37 *	−2.06
614.226	0	(o)	7/2	162,806	(e)	9/2	2.12×10^{9}	1.47×10^{9}	−0.92	−1.07
615.162	0	(o)	7/2	162,558	(e)	7/2	8.44×10^{8}	7.14×10^{8}	−1.32	−1.39
615.447	0	(o)	7/2	162,483	(e)	9/2	1.40×10^{8} *	6.17×10^{8}	−2.10 *	−1.45
617.384	0	(o)	7/2	161,973	(e)	5/2	7.39×10^{7} *	8.93×10^{7} #	−2.37 *	−2.29 #
618.330	11,793	(o)	5/2	173,520	(e)	7/2	4.18×10^{8} *	3.99×10^{8}	−1.62 *	−1.64
626.285	11,793	(o)	5/2	171,465	(e)	3/2	1.19×10^{8} *	1.12×10^{8}	−2.16 *	−2.18
628.091	11,793	(o)	5/2	171,005	(e)	5/2	3.33×10^{8}	9.45×10^{7}	−1.71	−2.25
628.793	0	(o)	7/2	159,035	(e)	7/2	7.29×10^{8} *	7.47×10^{8}	−1.37 *	−1.35
628.998	0	(o)	7/2	158,983	(e)	5/2	7.72×10^{7}	3.89×10^{7} #	−2.34	−2.62 #
637.437	11,793	(o)	5/2	168,671	(e)	7/2	1.03×10^{8} *	1.63×10^{8}	−2.20 *	−2.00
637.531	0	(o)	7/2	156,855	(e)	9/2	4.46×10^{8}	1.57×10^{8}	−1.57	−2.02
640.120	0	(o)	7/2	156,219	(e)	7/2	7.18×10^{7} *	1.41×10^{7} #	−2.36 *	−3.06 #
643.374	11,793	(o)	5/2	167,223	(e)	5/2	2.15×10^{8} *	6.96×10^{7}	−1.88 *	−2.37
645.219	0	(o)	7/2	154,985	(e)	9/2	2.86×10^{8}	4.81×10^{8}	−1.75	−1.51
646.060	11,793	(o)	5/2	166,577	(e)	5/2	1.01×10^{8} *	2.75×10^{8}	−2.20 *	−1.76
646.238	11,793	(o)	5/2	166,535	(e)	7/2	1.03×10^{8} *	5.21×10^{7} #	−2.19 *	−2.49 #

Table 1. *Cont.*

λ (Å) [a]	Lower Level [b]			Upper Level [b]			gA (s^{-1}) [c]		log gf [c]	
	E (cm^{-1})	(P)	J	E (cm^{-1})	(P)	J	HFR [d]	MCDHF [e]	HFR [d]	MCDHF [e]
647.581	0	(o)	7/2	154,421	(e)	5/2	2.66×10^{2} *	1.64×10^{6}	−7.77 *	−3.98
656.146	11,793	(o)	5/2	164,198	(e)	7/2	1.52×10^{8}	7.50×10^{7}	−2.01	−2.31
659.711	147,970	(e)	15/2	299,551	(o)	13/2	8.03×10^{5} *	8.85×10^{5} #	−4.29 *	−4.30 #
663.292	11,793	(o)	5/2	162,558	(e)	7/2	1.22×10^{8} *	2.18×10^{8}	−2.09 *	−1.84
664.182	0	(o)	7/2	150,561	(e)	7/2	1.23×10^{8} *	1.34×10^{8}	−2.09 *	−2.04
665.863	11,793	(o)	5/2	161,973	(e)	5/2	1.16×10^{7} *	1.51×10^{7}	−3.11 *	−2.99
699.848	156,663	(e)	15/2	299,551	(o)	13/2	3.58×10^{5} *	3.53×10^{5} #	−4.58 *	−4.65 #
701.121	11,793	(o)	5/2	154,421	(e)	5/2	2.59×10^{7} *	3.80×10^{7}	−2.72 *	−2.55
711.861	159,402	(e)	13/2	299,879	(o)	11/2	7.36×10^{4} *	8.15×10^{5} #	−5.25 *	−4.28 #
718.842	171,307	(e)	7/2	310,420	(o)	9/2	3.21×10^{7}	9.84×10^{7}	−2.60	−2.17
757.646	143,721	(e)	9/2	275,709	(o)	9/2	1.44×10^{8}	4.13×10^{8}	−1.89	−1.50
786.582	160,846	(e)	3/2	287,980	(o)	5/2	7.85×10^{7} *	2.09×10^{8}	−2.13 *	−1.77
790.958	143,721	(e)	9/2	270,150	(o)	11/2	1.16×10^{9}	1.64×10^{9}	−0.96	−0.86
791.571	154,985	(e)	9/2	281,316	(o)	11/2	3.38×10^{8}	8.23×10^{8}	−1.49	−1.15
793.168	143,721	(e)	9/2	269,797	(o)	9/2	1.02×10^{8} *	2.84×10^{7} #	−2.01 *	−2.62 #
798.330	162,806	(e)	9/2	288,068	(o)	9/2	6.79×10^{8}	7.94×10^{8}	−1.18	−1.17
798.984	162,909	(e)	11/2	288,068	(o)	9/2	5.63×10^{8}	8.03×10^{8}	−1.26	−1.16
803.460	156,855	(e)	9/2	281,316	(o)	11/2	1.22×10^{9}	9.96×10^{8}	−0.92	−1.05
804.510	157,016	(e)	13/2	281,316	(o)	11/2	5.71×10^{8}	7.00×10^{8}	−1.25	−1.21
804.715	143,721	(e)	9/2	267,988	(o)	11/2	1.12×10^{9}	3.63×10^{8}	−0.96	−1.50
805.483	151,786	(e)	13/2	275,935	(o)	11/2	8.48×10^{8}	1.09×10^{9}	−1.07	−1.02
806.043	160,846	(e)	3/2	284,908	(o)	5/2	5.67×10^{8}	1.06×10^{9}	−1.25	−1.03
807.412	150,561	(e)	7/2	274,413	(o)	5/2	5.23×10^{8}	3.44×10^{8}	−1.28	−1.53
808.779	162,558	(e)	7/2	286,201	(o)	9/2	1.94×10^{8} *	9.12×10^{7}	−1.71 *	−2.09
811.908	154,421	(e)	5/2	277,587	(o)	5/2	3.29×10^{7} *	7.04×10^{7}	−2.49 *	−2.21
813.433	161,973	(e)	5/2	284,908	(o)	5/2	4.34×10^{8}	5.82×10^{8}	−1.36	−1.28
814.355	157,016	(e)	13/2	279,813	(o)	13/2	9.82×10^{8}	9.72×10^{8}	−1.00	−1.05
817.741	147,970	(e)	15/2	270,258	(o)	13/2	2.36×10^{9}	2.18×10^{9}	−0.62	−0.70
818.952	166,535	(e)	7/2	288,642	(o)	7/2	3.86×10^{8}	3.40×10^{8}	−1.40	−1.51
819.642	164,198	(e)	7/2	286,201	(o)	9/2	2.64×10^{8}	6.54×10^{8}	−1.56	−1.23
820.249	159,402	(e)	13/2	281,316	(o)	11/2	2.06×10^{9}	1.78×10^{9}	−0.67	−0.79
821.643	148,551	(e)	11/2	270,258	(o)	13/2	5.15×10^{9}	5.44×10^{9}	−0.27	−0.30
821.750	163,804	(e)	13/2	285,495	(o)	11/2	7.95×10^{8} *	1.32×10^{9}	−1.09 *	−0.91
822.378	148,551	(e)	11/2	270,150	(o)	11/2	1.47×10^{8} *	3.97×10^{8}	−1.82 *	−1.44
822.497	154,985	(e)	9/2	276,567	(o)	7/2	8.08×10^{8} *	4.11×10^{8}	−2.08 *	−1.43
822.821	166,535	(e)	7/2	288,068	(o)	9/2	4.68×10^{8}	5.58×10^{8}	−1.31	−1.29
822.936	167,125	(e)	9/2	288,642	(o)	7/2	2.64×10^{8}	4.40×10^{8}	−1.56	−1.40
823.595	167,223	(e)	5/2	288,642	(o)	7/2	4.54×10^{8}	5.19×10^{8}	−1.33	−1.33
825.428	166,240	(e)	9/2	287,390	(o)	7/2	6.33×10^{8}	1.38×10^{9}	−1.18	−0.90
825.652	158,983	(e)	5/2	280,099	(o)	7/2	2.23×10^{9}	2.24×10^{9}	−0.63	−0.69
825.910	182,025	(e)	5/2	303,103	(o)	5/2	4.75×10^{8}	3.18×10^{8}	−1.31	−1.54
826.794	154,985	(e)	9/2	275,935	(o)	11/2	1.15×10^{9}	7.40×10^{8}	−0.92	−1.17
827.260	155,054	(e)	11/2	275,935	(o)	11/2	2.49×10^{9}	1.73×10^{9}	−0.58	−0.79
827.442	166,535	(e)	7/2	287,390	(o)	7/2	5.19×10^{8}	5.02×10^{8}	−1.26	−1.33
828.845	165,551	(e)	11/2	286,201	(o)	9/2	5.45×10^{8}	8.28×10^{8}	−1.24	−1.11
829.830	176,019	(e)	11/2	296,526	(o)	11/2	1.51×10^{9}	1.36×10^{9}	−0.80	−0.89
830.408	147,970	(e)	15/2	268,393	(o)	15/2	2.51×10^{9}	1.96×10^{9}	−0.58	−0.74
830.492	159,402	(e)	13/2	279,813	(o)	13/2	8.43×10^{8}	4.48×10^{8}	−1.05	−1.37
831.499	167,125	(e)	9/2	287,390	(o)	7/2	1.36×10^{9}	7.20×10^{8}	−0.84	−1.17
832.149	154,985	(e)	9/2	275,157	(o)	7/2	1.24×10^{9}	5.01×10^{8}	−0.89	−1.33
833.538	168,671	(e)	7/2	288,642	(o)	7/2	7.69×10^{8}	3.35×10^{8}	−1.09	−1.51
833.931	177,396	(e)	9/2	297,310	(o)	9/2	6.54×10^{8}	7.71×10^{8}	−1.15	−1.13
834.694	143,721	(e)	9/2	263,525	(o)	9/2	5.08×10^{8}	5.92×10^{8}	−1.27	−1.27
836.108	143,721	(e)	9/2	263,323	(o)	7/2	2.52×10^{8}	2.59×10^{8}	−1.58	−1.63
836.289	168,491	(e)	11/2	288,068	(o)	9/2	2.61×10^{9}	2.67×10^{9}	−0.55	−0.60
837.382	166,535	(e)	7/2	285,954	(o)	7/2	2.40×10^{6} *	1.05×10^{9}	−3.58 *	−0.99
838.674	150,561	(e)	7/2	269,797	(o)	9/2	2.13×10^{6} *	8.43×10^{8}	−3.63 *	−1.10
839.780	156,855	(e)	9/2	275,935	(o)	11/2	3.31×10^{8}	6.59×10^{8}	−1.44	−1.20
840.916	157,016	(e)	13/2	275,935	(o)	11/2	3.60×10^{9}	3.29×10^{9}	−0.41	−0.51
841.366	156,855	(e)	9/2	275,709	(o)	9/2	2.61×10^{8} *	6.26×10^{8}	−1.55 *	−1.22
841.544	167,125	(e)	9/2	285,954	(o)	7/2	2.25×10^{7} *	1.24×10^{9}	−2.61 *	−0.92
843.058	168,671	(e)	7/2	287,287	(o)	5/2	5.50×10^{8}	1.80×10^{8}	−1.22	−1.76
843.503	159,035	(e)	7/2	277,587	(o)	5/2	7.23×10^{7} *	1.65×10^{8}	−3.08 *	−1.81

Table 1. *Cont.*

	Lower Level [b]			Upper Level [b]			gA (s^{-1}) [c]		log gf [c]	
λ (Å) [a]	E (cm^{-1})	(P)	J	E (cm^{-1})	(P)	J	HFR [d]	MCDHF [e]	HFR [d]	MCDHF [e]
843.810	162,806	(e)	9/2	281,316	(o)	11/2	1.05×10^{9}	6.92×10^{8}	−0.94	−1.17
844.079	151,786	(e)	13/2	270,258	(o)	13/2	1.89×10^{9}	2.13×10^{9}	−0.69	−0.68
844.543	162,909	(e)	11/2	281,316	(o)	11/2	1.05×10^{9}	1.37×10^{9}	−0.94	−0.87
844.852	151,786	(e)	13/2	270,150	(o)	11/2	4.06×10^{8} *	9.00×10^{8}	−1.35 *	−1.06
845.296	156,855	(e)	9/2	275,157	(o)	7/2	2.09×10^{6} *	1.27×10^{7} #	−3.64 *	−2.91 #
846.067	156,219	(e)	7/2	274,413	(o)	5/2	4.55×10^{8}	3.72×10^{8}	−1.31	−1.45
847.460	162,806	(e)	9/2	280,805	(o)	9/2	2.83×10^{8} *	5.63×10^{8}	−1.50 *	−1.26
848.206	162,909	(e)	11/2	280,805	(o)	9/2	1.81×10^{9}	1.35×10^{9}	−0.70	−0.87
848.824	158,125	(e)	11/2	275,935	(o)	11/2	1.16×10^{9}	1.49×10^{9}	−0.89	−0.84
849.545	168,491	(e)	11/2	286,201	(o)	9/2	7.14×10^{8}	8.26×10^{8}	−1.10	−1.09
849.723	167,223	(e)	5/2	284,908	(o)	5/2	1.17×10^{9}	2.85×10^{8}	−0.89	−1.55
850.057	193,214	(e)	17/2	310,853	(o)	15/2	3.38×10^{10}	3.52×10^{10}	0.57	0.53
850.458	158,983	(e)	5/2	276,567	(o)	7/2	2.20×10^{8}	4.31×10^{7}	−1.62	−2.39
	158,125	(e)	11/2	275,709	(o)	9/2	7.59×10^{8}	4.04×10^{8}	−1.08	−1.40
850.836	159,035	(e)	7/2	276,567	(o)	7/2	7.50×10^{6} *	5.68×10^{8}	−3.08 *	−1.26
850.976	163,804	(e)	13/2	281,316	(o)	11/2	2.77×10^{8}	5.47×10^{8}	−1.51	−1.26
851.580	170,639	(e)	9/2	288,068	(o)	9/2	3.55×10^{9}	4.09×10^{9}	−0.40	−0.39
852.001	150,561	(e)	7/2	267,932	(o)	9/2	5.39×10^{9}	5.64×10^{9}	−0.23	−0.26
	185,736	(e)	7/2	303,103	(o)	5/2	6.13×10^{8}	1.77×10^{9}	−1.17	−0.76
852.267	171,307	(e)	7/2	288,642	(o)	7/2	1.11×10^{9}	9.69×10^{8}	−0.91	−1.03
852.709	180,036	(e)	7/2	297,310	(o)	9/2	1.41×10^{9}	1.25×10^{9}	−0.80	−0.90
853.379	156,219	(e)	7/2	273,400	(o)	9/2	5.94×10^{8}	3.87×10^{8}	−1.19	−1.42
855.408	162,909	(e)	11/2	279,813	(o)	13/2	1.15×10^{9}	9.32×10^{8} #	−0.89	−1.02 #
856.592	160,846	(e)	3/2	277,587	(o)	5/2	3.15×10^{8}	3.61×10^{8}	−1.46	−1.46
857.582	151,786	(e)	13/2	268,393	(o)	15/2	1.71×10^{9}	1.31×10^{9} #	−0.71	−0.88 #
	164,198	(e)	7/2	280,805	(o)	9/2	3.05×10^{9}	2.07×10^{9}	−0.46	−0.69
858.039	156,855	(e)	9/2	273,400	(o)	9/2	7.71×10^{8}	6.13×10^{8}	−1.07	−1.21
858.128	159,402	(e)	13/2	275,935	(o)	11/2	1.07×10^{9}	1.18×10^{9}	−0.92	−0.93
859.109	172,242	(e)	9/2	288,642	(o)	7/2	1.91×10^{9}	2.11×10^{9}	−0.67	−0.69
859.849	158,983	(e)	5/2	275,283	(o)	5/2	1.00×10^{9}	1.21×10^{9}	−0.96	−0.93
860.567	151,786	(e)	13/2	267,988	(o)	11/2	2.35×10^{9}	1.97×10^{9}	−0.58	−0.70
860.781	158,983	(e)	5/2	275,157	(o)	7/2	2.11×10^{9}	2.15×10^{9}	−0.62	−0.68
861.164	159,035	(e)	7/2	275,157	(o)	7/2	2.01×10^{9}	1.07×10^{9}	−0.64	−0.97
861.455	171,307	(e)	7/2	287,390	(o)	7/2	9.56×10^{8}	1.86×10^{9}	−0.96	−0.73
861.924	152,373	(e)	17/2	268,393	(o)	15/2	3.27×10^{10}	3.36×10^{10}	0.57	0.53
862.222	171,307	(e)	7/2	287,287	(o)	5/2	3.52×10^{9}	4.33×10^{9}	−0.40	−0.36
862.798	164,198	(e)	7/2	280,099	(o)	7/2	1.26×10^{9}	1.47×10^{9}	−0.84	−0.83
863.370	172,242	(e)	9/2	288,068	(o)	9/2	2.30×10^{8}	1.80×10^{8}	−1.58	−1.74
866.324	158,983	(e)	5/2	274,413	(o)	5/2	1.29×10^{9}	5.88×10^{8}	−0.83	−1.24
866.928	164,463	(e)	15/2	279,813	(o)	13/2	2.85×10^{10}	2.89×10^{10}	0.52	0.47
867.487	158,125	(e)	11/2	273,400	(o)	9/2	1.22×10^{8} *	9.24×10^{8}	−1.86 *	−1.03
868.023	155,054	(e)	11/2	270,258	(o)	13/2	1.40×10^{9}	1.40×10^{9}	−0.79	−0.84
868.327	154,985	(e)	9/2	270,150	(o)	11/2	7.81×10^{8}	2.30×10^{9}	−1.05	−0.63
868.447	172,242	(e)	9/2	287,390	(o)	7/2	2.02×10^{9}	1.95×10^{9}	−0.63	−0.70
868.652	173,520	(e)	7/2	288,642	(o)	7/2	1.17×10^{9}	2.15×10^{9}	−0.87	−0.66
868.841	172,885	(e)	5/2	287,980	(o)	5/2	1.04×10^{9}	6.06×10^{7}	−0.92	−2.21
	155,054	(e)	11/2	270,150	(o)	11/2	2.00×10^{9}	4.91×10^{9}	−0.64	−0.30
868.993	166,240	(e)	9/2	281,316	(o)	11/2	1.82×10^{9}	2.19×10^{9}	−0.67	−0.65
869.347	162,558	(e)	7/2	277,587	(o)	5/2	3.73×10^{8}	1.37×10^{8}	−1.37	−1.87
869.760	148,551	(e)	11/2	263,525	(o)	9/2	1.11×10^{9}	1.03×10^{9}	−0.90	−0.99
869.949	171,005	(e)	5/2	285,954	(o)	7/2	8.89×10^{8}	2.07×10^{9}	−0.99	−0.67
870.436	170,023	(e)	5/2	284,908	(o)	5/2	3.43×10^{8}	3.18×10^{9}	−1.40	−0.48
870.836	189,188	(e)	7/2	304,021	(o)	7/2	7.51×10^{8}	2.86×10^{8}	−1.06	−1.53
870.990	154,985	(e)	9/2	269,797	(o)	9/2	5.30×10^{0} *	5.26×10^{8}	−9.21 *	−1.27
	181,894	(e)	7/2	296,706	(o)	7/2	7.02×10^{9}	6.94×10^{9}	−0.08	−0.14
872.194	161,055	(e)	11/2	275,709	(o)	9/2	3.39×10^{9}	6.90×10^{9}	−0.40	−0.15
872.647	161,973	(e)	5/2	276,567	(o)	7/2	2.62×10^{8}	1.26×10^{9}	−1.52	−0.89
872.869	166,240	(e)	9/2	280,805	(o)	9/2	3.15×10^{9}	5.83×10^{9}	−0.43	−0.22
873.323	172,885	(e)	5/2	287,390	(o)	7/2	1.25×10^{9}	1.38×10^{9}	−0.83	−0.85
873.840	158,983	(e)	5/2	273,421	(o)	7/2	2.76×10^{9}	3.92×10^{9}	−0.50	−0.40
874.237	159,035	(e)	7/2	273,421	(o)	7/2	7.85×10^{8}	7.96×10^{8}	−1.05	−1.09
874.319	198,972	(e)	9/2	313,347	(o)	11/2	7.06×10^{9}	6.97×10^{9}	−0.08	−0.15

Table 1. *Cont.*

	Lower Level [b]			Upper Level [b]			gA (s^{-1}) [c]		log gf [c]	
λ (Å) [a]	E (cm^{-1})	(P)	J	E (cm^{-1})	(P)	J	HFR [d]	MCDHF [e]	HFR [d]	MCDHF [e]
874.638	181,894	(e)	7/2	296,226	(o)	5/2	1.45×10^9	1.84×10^9	−0.77	−1.72
875.121	166,535	(e)	7/2	280,805	(o)	9/2	1.21×10^9	6.93×10^8	−0.84	−1.13
875.645	182,025	(e)	5/2	296,226	(o)	5/2	4.35×10^9	4.58×10^9	−0.28	−0.31
875.724	167,125	(e)	9/2	281,316	(o)	11/2	1.00×10^9	1.36×10^8	−0.93	−1.85
875.892	182,357	(e)	13/2	296,526	(o)	11/2	2.41×10^{10}	2.42×10^{10}	0.45	0.40
876.449	174,544	(e)	9/2	288,642	(o)	7/2	4.57×10^8 *	2.59×10^8	−1.27 *	−1.58
876.548	162,483	(e)	9/2	276,567	(o)	7/2	3.61×10^8	4.24×10^9	−1.38	−0.36
877.127	162,558	(e)	7/2	276,567	(o)	7/2	5.78×10^7 *	2.63×10^8	−2.17 *	−1.57
877.501	172,242	(e)	9/2	286,201	(o)	9/2	3.39×10^9	4.81×10^9	−0.40	−0.30
877.848	189,188	(e)	7/2	303,103	(o)	5/2	9.81×10^9	8.98×10^9	0.07	−0.03
877.933	171,005	(e)	5/2	284,908	(o)	5/2	3.48×10^9	1.34×10^9	−0.38	−0.85
878.199	173,520	(e)	7/2	287,390	(o)	7/2	9.46×10^8	6.49×10^8	−0.95	−1.17
878.279	166,240	(e)	9/2	280,099	(o)	7/2	1.86×10^8 *	4.60×10^8	−1.66 *	−1.32
879.409	172,242	(e)	9/2	285,954	(o)	7/2	1.89×10^7 *	5.85×10^9	−2.65 *	−0.21
879.666	167,125	(e)	9/2	280,805	(o)	9/2	3.26×10^9	1.10×10^9	−0.41	−0.93
880.316	156,663	(e)	15/2	270,258	(o)	13/2	1.80×10^{10}	1.77×10^{10}	0.33	0.27
880.457	156,219	(e)	7/2	269,797	(o)	9/2	1.61×10^8	1.08×10^8	−1.72	−1.94
880.543	166,535	(e)	7/2	280,099	(o)	7/2	5.51×10^9	4.98×10^9	−0.18	−0.27
	160,846	(e)	3/2	274,413	(o)	5/2	4.44×10^9	3.84×10^9	−0.28	−0.40
880.610	161,973	(e)	5/2	275,530	(o)	3/2	7.55×10^8	7.48×10^8	−1.06	−1.12
880.873	174,544	(e)	9/2	288,068	(o)	9/2	2.73×10^9	2.10×10^9	−0.49	−0.66
881.434	162,483	(e)	9/2	275,935	(o)	11/2	7.92×10^8	6.92×10^8	−1.02	−1.14
881.497	171,465	(e)	3/2	284,908	(o)	5/2	3.81×10^9	3.57×10^9	−0.34	−0.42
882.537	161,973	(e)	5/2	275,283	(o)	5/2	5.39×10^8	4.41×10^8	−1.20	−1.34
882.654	156,855	(e)	9/2	270,150	(o)	11/2	3.90×10^8	4.61×10^8	−1.33	−1.31
882.963	172,242	(e)	9/2	285,495	(o)	11/2	5.55×10^8	5.07×10^8	−1.17	−1.27
883.065	157,016	(e)	13/2	270,258	(o)	13/2	6.32×10^9	6.04×10^9	−0.12	−0.20
883.520	161,973	(e)	5/2	275,157	(o)	7/2	2.44×10^9	1.69×10^9	−0.54	−0.75
883.609	174,895	(e)	7/2	288,068	(o)	9/2	2.78×10^8	2.64×10^8	−1.48	−1.55
883.914	157,016	(e)	13/2	270,150	(o)	11/2	1.98×10^7 *	1.18×10^9	−2.62 *	−0.91
884.111	164,479	(e)	3/2	277,587	(o)	5/2	9.11×10^7	3.62×10^8	−1.96	−1.43
884.207	184,215	(e)	11/2	297,310	(o)	9/2	1.36×10^{10}	1.37×10^{10}	0.22	0.16
884.290	174,895	(e)	7/2	287,980	(o)	5/2	1.08×10^9	1.91×10^9	−0.88	−0.70
	171,307	(e)	7/2	284,393	(o)	9/2	5.01×10^7 *	5.51×10^7	−2.23 *	−2.23
884.512	183,649	(e)	9/2	296,706	(o)	7/2	6.39×10^9	6.35×10^9	−0.11	−0.17
884.747	190,994	(e)	5/2	304,021	(o)	7/2	1.91×10^8	1.92×10^8	−1.64	−1.70
884.928	154,985	(e)	9/2	267,988	(o)	11/2	1.51×10^9	1.22×10^9	−0.75	−0.89
885.057	175,654	(e)	7/2	288,642	(o)	7/2	1.11×10^9	7.33×10^8	−0.88	−1.11
885.160	167,125	(e)	9/2	280,099	(o)	7/2	2.43×10^8 *	5.04×10^7 #	−1.53 *	−2.27 #
885.235	150,561	(e)	7/2	263,525	(o)	9/2	2.96×10^9	3.67×10^9	−0.46	−0.42
885.394	156,855	(e)	9/2	269,797	(o)	9/2	4.56×10^7 *	1.29×10^9	−2.26 *	−0.86
885.720	162,806	(e)	9/2	275,709	(o)	9/2	4.85×10^7 *	4.49×10^8	−2.23 *	−1.33
885.923	183,649	(e)	9/2	296,526	(o)	11/2	9.45×10^8	7.70×10^8 #	−0.94	−1.08 #
886.160	143,721	(e)	9/2	256,566	(o)	11/2	1.41×10^{10}	1.58×10^{10}	0.22	0.21
	174,544	(e)	9/2	287,390	(o)	7/2	9.68×10^9	9.37×10^9	0.07	0.00
886.322	168,491	(e)	11/2	281,316	(o)	11/2	8.07×10^9	7.82×10^9	−0.01	−0.08
886.438	168,506	(e)	13/2	281,316	(o)	11/2	1.47×10^{10}	1.42×10^{10}	0.25	0.18
886.533	162,909	(e)	11/2	275,709	(o)	9/2	1.03×10^9	1.53×10^9	−0.90	−0.79
886.824	150,561	(e)	7/2	263,323	(o)	7/2	3.79×10^9	3.33×10^9	−0.35	−0.47
887.517	162,483	(e)	9/2	275,157	(o)	7/2	7.37×10^9	2.95×10^9	−0.05	−0.51
888.110	162,558	(e)	7/2	275,157	(o)	7/2	5.19×10^9	5.54×10^9	−0.21	−0.23
888.932	174,895	(e)	7/2	287,390	(o)	7/2	1.92×10^9	1.85×10^9	−0.63	−0.70
889.359	161,973	(e)	5/2	274,413	(o)	5/2	1.98×10^9	2.18×10^9	−0.62	−0.64
889.410	173,520	(e)	7/2	285,954	(o)	7/2	1.89×10^4 *	1.57×10^9	−5.64 *	−0.77
889.923	164,198	(e)	7/2	276,567	(o)	7/2	1.92×10^9	1.74×10^9	−0.64	−0.74
890.068	162,806	(e)	9/2	275,157	(o)	7/2	2.22×10^8	3.13×10^9	−1.57	−0.48
890.114	161,055	(e)	11/2	273,400	(o)	9/2	1.00×10^{10}	6.44×10^9	0.08	−0.16
890.360	168,491	(e)	11/2	280,805	(o)	9/2	8.28×10^9	8.48×10^9	0.01	−0.04
891.814	163,804	(e)	13/2	275,935	(o)	11/2	1.81×10^{10}	1.77×10^{10}	0.34	0.28
891.991	190,994	(e)	5/2	303,103	(o)	5/2	3.21×10^9	3.14×10^9	−0.41	−0.47
892.556	201,310	(e)	11/2	313,347	(o)	11/2	3.44×10^8	6.52×10^9	−1.38	−0.15

Table 1. *Cont.*

	Lower Level [b]			Upper Level [b]			gA (s^{-1}) [c]		log gf [c]	
λ (Å) [a]	E (cm^{-1})	(P)	J	E (cm^{-1})	(P)	J	HFR [d]	MCDHF [e]	HFR [d]	MCDHF [e]
892.656	158,125	(e)	11/2	270,150	(o)	11/2	2.18×10^{9}	3.23×10^{9}	−0.57	−0.46
	187,526	(e)	15/2	299,551	(o)	13/2	2.39×10^{10}	2.71×10^{10}	0.45	0.45
893.489	192,100	(e)	9/2	304,021	(o)	7/2	1.60×10^{10}	1.61×10^{10}	0.30	0.24
894.013	162,558	(e)	7/2	274,413	(o)	5/2	2.34×10^{9}	2.10×10^{9}	−0.54	−0.65
895.014	156,663	(e)	15/2	268,393	(o)	15/2	9.30×10^{9}	9.46×10^{9}	0.06	0.02
895.152	156,219	(e)	7/2	267,932	(o)	9/2	6.94×10^{9}	6.23×10^{9}	−0.08	−0.17
895.470	158,125	(e)	11/2	269,797	(o)	9/2	4.04×10^{8}	2.31×10^{9}	−1.31	−0.60
897.282	161,973	(e)	5/2	273,421	(o)	7/2	2.80×10^{9}	2.70×10^{9}	−0.47	−0.54
	198,972	(e)	9/2	310,420	(o)	9/2	9.60×10^{9}	9.79×10^{9}	0.08	0.03
897.422	168,671	(e)	7/2	280,099	(o)	7/2	2.55×10^{8}	5.16×10^{8}	−1.50	−1.24
897.766	173,520	(e)	7/2	284,908	(o)	5/2	1.26×10^{9}	1.46×10^{9}	−0.81	−0.79
897.857	157,016	(e)	13/2	268,393	(o)	15/2	5.63×10^{8}	4.44×10^{8} #	−1.16	−1.31 #
898.301	168,491	(e)	11/2	279,813	(o)	13/2	7.09×10^{8}	5.11×10^{8} #	−1.05	−1.25 #
898.415	168,506	(e)	13/2	279,813	(o)	13/2	8.10×10^{9}	7.96×10^{9}	0.01	−0.05
898.918	177,396	(e)	9/2	288,642	(o)	7/2	4.54×10^{9}	2.54×10^{9}	−0.25	−0.57
898.980	176,831	(e)	11/2	288,068	(o)	9/2	1.59×10^{10}	1.58×10^{10}	0.30	0.24
899.489	202,173	(e)	11/2	313,347	(o)	11/2	1.25×10^{10}	7.02×10^{9}	−0.71	−0.11
899.817	156,855	(e)	9/2	267,988	(o)	11/2	2.42×10^{9}	9.66×10^{8}	−0.53	−0.97
900.213	164,198	(e)	7/2	275,283	(o)	5/2	1.64×10^{9}	9.93×10^{8}	−0.70	−0.98
900.271	156,855	(e)	9/2	267,932	(o)	9/2	7.55×10^{9}	4.84×10^{9}	−0.03	−0.27
900.812	166,577	(e)	5/2	277,587	(o)	5/2	9.59×10^{8}	1.71×10^{8}	−0.93	−1.74
901.126	157,016	(e)	13/2	267,988	(o)	11/2	1.22×10^{10}	1.25×10^{10}	0.17	0.13
901.232	164,198	(e)	7/2	275,157	(o)	7/2	6.54×10^{6} *	7.98×10^{5} #	−3.09 *	−4.07 #
901.582	162,483	(e)	9/2	273,400	(o)	9/2	3.62×10^{9}	1.33×10^{9}	−0.36	−0.84
902.185	162,558	(e)	7/2	273,400	(o)	9/2	1.37×10^{9}	5.60×10^{8}	−0.78	−1.22
902.499	164,479	(e)	3/2	275,283	(o)	5/2	2.98×10^{9}	2.90×10^{9}	−0.44	−0.51
902.833	203,211	(e)	15/2	313,974	(o)	13/2	1.60×10^{10}	1.56×10^{10}	0.30	0.24
902.954	159,402	(e)	13/2	270,150	(o)	11/2	1.48×10^{10}	1.10×10^{10}	0.27	0.08
904.594	175,654	(e)	7/2	286,201	(o)	9/2	3.44×10^{8}	6.51×10^{8}	−1.36	−1.13
905.047	162,909	(e)	11/2	273,400	(o)	9/2	5.55×10^{8}	4.20×10^{8}	−1.16	−1.33
906.082	167,223	(e)	5/2	277,587	(o)	5/2	6.45×10^{8}	1.55×10^{9}	−1.09	−0.77
906.619	175,654	(e)	7/2	285,954	(o)	7/2	2.54×10^{8} *	1.63×10^{9}	−1.49 *	−0.73
907.554	203,161	(e)	13/2	313,347	(o)	11/2	9.02×10^{9}	8.47×10^{9}	0.06	−0.02
907.718	170,639	(e)	9/2	280,805	(o)	9/2	2.30×10^{9}	1.40×10^{9}	−0.53	−0.79
908.460	170,023	(e)	5/2	280,099	(o)	7/2	1.06×10^{9}	7.55×10^{8}	−0.87	−1.07
908.988	178,629	(e)	9/2	288,642	(o)	7/2	8.44×10^{9}	1.02×10^{10}	0.03	0.06
909.637	164,479	(e)	3/2	274,413	(o)	5/2	7.91×10^{8}	1.16×10^{9}	−1.00	−0.89
909.941	177,390	(e)	5/2	287,287	(o)	5/2	4.22×10^{8}	8.32×10^{7}	−1.27	−2.03
910.156	181,894	(e)	7/2	291,764	(o)	5/2	1.89×10^{9}	3.05×10^{9}	−0.64	−0.49
910.220	158,125	(e)	11/2	267,988	(o)	11/2	6.20×10^{9}	3.15×10^{9}	−0.11	−0.45
910.683	158,125	(e)	11/2	267,932	(o)	9/2	4.78×10^{9}	3.48×10^{9}	−0.22	−0.41
911.242	182,025	(e)	5/2	291,764	(o)	5/2	5.07×10^{8}	1.09×10^{8} #	−1.20	−1.92 #
911.509	182,025	(e)	5/2	291,733	(o)	3/2	1.69×10^{9}	1.34×10^{9}	−0.68	−0.83
912.834	195,441	(e)	5/2	304,990	(o)	5/2	2.27×10^{9}	2.73×10^{9}	−0.55	−0.52
913.569	170,639	(e)	9/2	280,099	(o)	7/2	4.32×10^{9}	4.30×10^{9}	−0.25	−0.30
913.729	167,125	(e)	9/2	276,567	(o)	7/2	4.30×10^{9}	1.84×10^{9}	−0.26	−0.69
914.012	186,818	(e)	5/2	296,226	(o)	5/2	2.72×10^{8}	3.22×10^{8}	−1.45	−1.43
914.326	176,831	(e)	11/2	286,201	(o)	9/2	8.56×10^{8}	5.34×10^{8}	−0.95	−1.21
914.719	147,970	(e)	15/2	257,293	(o)	13/2	2.21×10^{10}	2.44×10^{10}	0.44	0.43
915.730	164,198	(e)	7/2	273,400	(o)	9/2	5.04×10^{8}	1.04×10^{9}	−1.20	−0.94
	161,055	(e)	11/2	270,258	(o)	13/2	8.65×10^{7}	7.62×10^{7} #	−1.95	−2.06 #
916.503	201,310	(e)	11/2	310,420	(o)	9/2	1.31×10^{8} *	1.75×10^{9}	−1.77 *	−0.69
917.821	166,577	(e)	5/2	275,530	(o)	3/2	1.12×10^{9}	6.51×10^{6} #	−0.85	−3.14 #
918.131	166,240	(e)	9/2	275,157	(o)	7/2	2.34×10^{6} *	3.19×10^{8}	−3.52 *	−1.45
918.260	154,421	(e)	5/2	263,323	(o)	7/2	7.01×10^{9}	7.17×10^{9}	−0.05	−0.10
919.071	177,396	(e)	9/2	286,201	(o)	9/2	3.62×10^{8}	1.40×10^{8}	−1.33	−1.79
919.557	166,535	(e)	7/2	275,283	(o)	5/2	2.33×10^{9}	3.09×10^{9}	−0.53	−0.46
919.607	148,551	(e)	11/2	257,293	(o)	13/2	3.36×10^{9}	3.25×10^{9}	−0.37	−0.44
919.909	166,577	(e)	5/2	275,283	(o)	5/2	2.33×10^{9}	9.97×10^{8}	−0.53	−0.95
920.269	176,831	(e)	11/2	285,495	(o)	11/2	7.09×10^{8}	7.06×10^{8}	−1.03	−1.08
920.621	166,535	(e)	7/2	275,157	(o)	7/2	1.70×10^{8}	3.73×10^{8}	−1.65	−1.37
920.925	159,402	(e)	13/2	267,988	(o)	11/2	1.68×10^{9}	5.87×10^{9}	−0.67	−0.17
921.116	172,242	(e)	9/2	280,805	(o)	9/2	3.85×10^{8}	4.09×10^{8}	−1.30	−1.32

Table 1. *Cont.*

λ (Å) [a]	Lower Level [b] E (cm^{-1})	(P)	J	Upper Level [b] E (cm^{-1})	(P)	J	gA (s^{-1}) [c] HFR [d]	gA (s^{-1}) [c] MCDHF [e]	log gf [c] HFR [d]	log gf [c] MCDHF [e]
921.319	154,985	(e)	9/2	263,525	(o)	9/2	6.60×10^9	6.09×10^9	−0.08	−0.17
921.898	155,054	(e)	11/2	263,525	(o)	9/2	1.15×10^{10}	1.07×10^{10}	0.17	0.08
922.727	176,019	(e)	11/2	284,393	(o)	9/2	5.51×10^9	1.06×10^{10}	−0.15	0.08
923.042	154,985	(e)	9/2	263,323	(o)	7/2	3.50×10^9	2.45×10^9	−0.35	−0.56
923.492	196,706	(e)	5/2	304,990	(o)	5/2	5.80×10^8	1.87×10^8	−1.13	−1.67
923.812	202,173	(e)	11/2	310,420	(o)	9/2	3.73×10^9	1.79×10^9	−0.31	−0.68
925.408	167,223	(e)	5/2	275,283	(o)	5/2	2.52×10^8	1.83×10^9	−1.49	−0.68
925.655	167,125	(e)	9/2	275,157	(o)	7/2	1.75×10^8 *	1.46×10^9	−1.64 *	−0.78
925.787	148,551	(e)	11/2	256,566	(o)	11/2	9.95×10^9	1.10×10^{10}	0.11	0.10
926.489	167,223	(e)	5/2	275,157	(o)	7/2	1.49×10^8	8.72×10^8	−1.71	−0.99
926.815	168,671	(e)	7/2	276,567	(o)	7/2	1.37×10^8	3.45×10^8	−1.74	−1.40
926.999	177,396	(e)	9/2	285,271	(o)	7/2	4.06×10^6 *	4.26×10^9	−3.27 *	−0.30
927.222	165,551	(e)	11/2	273,400	(o)	9/2	4.39×10^9	9.01×10^9	−0.24	0.02
929.005	203,211	(e)	15/2	310,853	(o)	15/2	9.66×10^9	9.64×10^9 #	0.11	0.06 #
929.606	178,629	(e)	9/2	286,201	(o)	9/2	3.61×10^9	2.53×10^9	−0.32	−0.52
929.670	170,023	(e)	5/2	277,587	(o)	5/2	1.98×10^9	5.06×10^8	−0.58	−1.24
931.584	162,806	(e)	9/2	270,150	(o)	11/2	2.81×10^9	2.14×10^9	−0.43	−0.60
931.917	156,219	(e)	7/2	263,525	(o)	9/2	4.16×10^8	5.04×10^8	−1.27	−1.24
932.915	167,223	(e)	5/2	274,413	(o)	5/2	4.10×10^8	1.01×10^8	−1.26	−1.93
933.007	166,240	(e)	9/2	273,421	(o)	7/2	2.97×10^9	1.55×10^9	−0.41	−0.74
933.182	166,240	(e)	9/2	273,400	(o)	9/2	2.15×10^9	1.43×10^9	−0.55	−0.78
933.672	156,219	(e)	7/2	263,323	(o)	7/2	3.57×10^9	4.48×10^9	−0.33	−0.29
934.647	162,806	(e)	9/2	269,797	(o)	9/2	6.69×10^9	4.95×10^9	−0.05	−0.23
935.448	198,089	(e)	7/2	304,990	(o)	5/2	5.38×10^9	4.42×10^9	−0.15	−0.30
935.559	162,909	(e)	11/2	269,797	(o)	9/2	4.46×10^9	3.02×10^9	−0.22	−0.44
937.466	156,855	(e)	9/2	263,525	(o)	9/2	8.31×10^8	2.05×10^9	−0.96	−0.62
937.713	178,629	(e)	9/2	285,271	(o)	7/2	1.68×10^8 *	7.58×10^8	−1.64 *	−1.04
938.578	170,023	(e)	5/2	276,567	(o)	7/2	6.32×10^8	3.89×10^8	−1.07	−1.34
939.097	168,671	(e)	7/2	275,157	(o)	7/2	2.93×10^8	3.17×10^7 #	−1.40	−2.42 #
940.328	163,804	(e)	13/2	270,150	(o)	11/2	3.36×10^8	3.96×10^8	−1.34	−1.32
940.775	167,125	(e)	9/2	273,421	(o)	7/2	1.00×10^9	2.57×10^9	−0.88	−0.52
941.636	167,223	(e)	5/2	273,421	(o)	7/2	1.88×10^9	1.14×10^9	−0.60	−0.87
947.805	151,786	(e)	13/2	257,293	(o)	13/2	9.74×10^9	1.03×10^{10}	0.12	0.09
948.762	158,125	(e)	11/2	263,525	(o)	9/2	1.64×10^9	2.83×10^9	−0.65	−0.47
950.032	170,023	(e)	5/2	275,283	(o)	5/2	1.28×10^9	3.95×10^8	−0.76	−1.33
950.246	180,036	(e)	7/2	285,271	(o)	7/2	4.67×10^8	5.21×10^9	−1.19	−0.19
950.729	162,806	(e)	9/2	267,988	(o)	11/2	7.93×10^7 *	5.22×10^8	−1.97 *	−1.20
951.237	162,806	(e)	9/2	267,932	(o)	9/2	4.63×10^7 *	1.42×10^9	−2.20 *	−0.76
951.662	162,909	(e)	11/2	267,988	(o)	11/2	1.65×10^9	4.43×10^9	−0.64	−0.26
952.173	162,909	(e)	11/2	267,932	(o)	9/2	2.05×10^8 *	1.62×10^9	−1.55 *	−0.70
952.873	186,818	(e)	5/2	291,764	(o)	5/2	2.70×10^9	2.80×10^9	−0.44	−0.48
953.165	186,818	(e)	5/2	291,733	(o)	3/2	1.58×10^9	1.45×10^9	−0.68	−0.77
954.374	151,786	(e)	13/2	256,566	(o)	11/2	5.49×10^9	5.57×10^9	−0.13	−0.17
956.772	170,639	(e)	9/2	275,157	(o)	7/2	8.14×10^7 *	1.22×10^9	−1.94 *	−0.82
958.970	171,005	(e)	5/2	275,283	(o)	5/2	2.17×10^8	1.19×10^9	−1.52	−0.84
960.921	173,520	(e)	7/2	277,587	(o)	5/2	1.93×10^9	2.36×10^9	−0.57	−0.54
963.227	171,465	(e)	3/2	275,283	(o)	5/2	9.93×10^8	1.33×10^9	−0.86	−0.79
965.653	166,240	(e)	9/2	269,797	(o)	9/2	7.30×10^8	1.13×10^9	−0.98	−0.85
974.890	189,188	(e)	7/2	291,764	(o)	5/2	9.79×10^8	5.43×10^8	−0.85	−1.16
	197,304	(e)	13/2	299,879	(o)	11/2	5.16×10^9	4.92×10^9	−0.13	−0.19
978.015	197,304	(e)	13/2	299,551	(o)	13/2	8.87×10^9	9.56×10^9	0.11	0.10
979.306	171,307	(e)	7/2	273,421	(o)	7/2	1.44×10^9	1.22×10^9	−0.68	−0.80
1002.891	156,855	(e)	9/2	256,566	(o)	11/2	7.45×10^8	8.86×10^8	−0.95	−0.92
1008.394	158,125	(e)	11/2	257,293	(o)	13/2	6.14×10^8	6.54×10^8	−1.03	−1.05
1015.829	158,125	(e)	11/2	256,566	(o)	11/2	5.73×10^8	6.75×10^8	−1.05	−1.03
1236.607	187,526	(e)	15/2	268,393	(o)	15/2	1.76×10^4 *	9.56×10^3 #	−5.38 *	−5.68 #
1247.456	217,147	(e)	7/2	297,310	(o)	9/2	1.10×10^7 *	1.39×10^7	−2.57 *	−2.48
1290.447	207,779	(e)	7/2	285,271	(o)	7/2	2.83×10^7 *	5.16×10^5 #	−2.15 *	−3.88 #
1420.023	243,552	(e)	11/2	313,974	(o)	13/2	5.36×10^9	5.00×10^9	0.23	0.18
1429.209	217,422	(e)	9/2	287,390	(o)	7/2	4.96×10^6 *	3.62×10^4 #	−2.81 *	−4.96 #
1432.500	243,539	(e)	13/2	313,347	(o)	11/2	2.51×10^9	2.15×10^9	−0.09	−0.18
	207,779	(e)	7/2	277,587	(o)	5/2	1.78×10^9	2.49×10^9	−0.26	−0.12

Table 1. *Cont.*

λ (Å) [a]	Lower Level [b]			Upper Level [b]			gA (s^{-1}) [c]		log gf [c]	
	E (cm^{-1})	(P)	J	E (cm^{-1})	(P)	J	HFR [d]	MCDHF [e]	HFR [d]	MCDHF [e]
1432.771	243,552	(e)	11/2	313,347	(o)	11/2	1.46×10^{10}	1.54×10^{10}	0.67	0.67
1435.556	218,982	(e)	5/2	288,642	(o)	7/2	2.21×10^{9}	1.21×10^{9}	−0.15	−0.43
1441.761	211,957	(e)	11/2	281,316	(o)	11/2	1.12×10^{10}	1.14×10^{10}	0.56	0.56
1441.952	207,216	(e)	9/2	276,567	(o)	7/2	4.50×10^{7} *	1.61×10^{9}	−1.83 *	−0.29
1443.641	212,047	(e)	9/2	281,316	(o)	11/2	5.57×10^{9}	5.16×10^{9}	0.26	0.21
1448.138	217,147	(e)	7/2	286,201	(o)	9/2	3.46×10^{9}	4.37×10^{9}	0.06	0.14
1449.324	218,982	(e)	5/2	287,980	(o)	5/2	2.93×10^{8}	3.94×10^{4} #	−1.02	−4.90 #
1450.356	201,310	(e)	11/2	270,258	(o)	13/2	6.31×10^{9}	3.27×10^{9}	0.32	0.02
1450.686	228,377	(e)	7/2	297,310	(o)	9/2	5.15×10^{9}	4.96×10^{9}	0.23	0.20
1452.469	211,957	(e)	11/2	280,805	(o)	9/2	2.51×10^{9}	2.19×10^{9}	−0.08	−0.15
1452.638	201,310	(e)	11/2	270,150	(o)	11/2	7.11×10^{9}	6.27×10^{9}	0.37	0.30
1453.353	219,261	(e)	7/2	288,068	(o)	9/2	1.33×10^{10}	1.30×10^{10}	0.64	0.62
1453.751	207,779	(e)	7/2	276,567	(o)	7/2	9.94×10^{8}	4.73×10^{9}	−0.50	0.18
1453.910	217,422	(e)	9/2	286,201	(o)	9/2	5.42×10^{9}	7.26×10^{9}	0.25	0.37
1454.375	212,047	(e)	9/2	280,805	(o)	9/2	1.09×10^{10}	1.09×10^{10}	0.56	0.55
1455.214	207,216	(e)	9/2	275,935	(o)	11/2	1.47×10^{9}	1.57×10^{10}	−0.30	0.70
	219,261	(e)	7/2	287,980	(o)	5/2	7.04×10^{8}	8.94×10^{7}	−0.63	−1.55
1459.156	217,422	(e)	9/2	285,954	(o)	7/2	1.96×10^{7} *	2.06×10^{9}	−2.19 *	−0.17
1460.113	201,310	(e)	11/2	269,797	(o)	9/2	3.64×10^{9}	4.63×10^{9}	0.08	0.18
1460.708	220,182	(e)	5/2	288,642	(o)	7/2	8.12×10^{9}	9.14×10^{9}	0.43	0.47
1461.825	218,982	(e)	5/2	287,390	(o)	7/2	4.63×10^{9}	4.81×10^{9}	0.19	0.20
1463.514	228,377	(e)	7/2	296,706	(o)	7/2	8.58×10^{9}	8.47×10^{9}	0.46	0.44
1464.031	218,982	(e)	5/2	287,287	(o)	5/2	4.67×10^{9}	5.23×10^{9}	0.20	0.23
1467.809	219,261	(e)	7/2	287,390	(o)	7/2	5.60×10^{9}	5.44×10^{9}	0.28	0.25
1468.749	202,173	(e)	11/2	270,258	(o)	13/2	1.24×10^{8}	2.72×10^{9}	−1.37	−0.05
	219,202	(e)	3/2	287,287	(o)	5/2	1.91×10^{9}	5.06×10^{8}	−0.19	−0.77
1468.991	217,422	(e)	9/2	285,495	(o)	11/2	1.62×10^{10}	1.56×10^{10}	0.74	0.71
1469.454	212,047	(e)	9/2	280,099	(o)	7/2	8.76×10^{9}	7.78×10^{9}	0.47	0.41
1470.045	219,261	(e)	7/2	287,287	(o)	5/2	1.39×10^{9}	1.96×10^{9}	−0.33	−0.19
1471.094	202,173	(e)	11/2	270,150	(o)	11/2	1.37×10^{8}	5.31×10^{9}	−1.32	0.24
1471.203	228,554	(e)	9/2	296,526	(o)	11/2	1.60×10^{10}	1.56×10^{10}	0.73	0.71
1471.880	207,216	(e)	9/2	275,157	(o)	7/2	1.92×10^{8}	1.14×10^{9}	−1.19	−0.43
1472.120	207,779	(e)	7/2	275,709	(o)	9/2	3.56×10^{9}	5.14×10^{9}	0.08	0.23
1473.710	211,957	(e)	11/2	279,813	(o)	13/2	1.89×10^{10}	1.82×10^{10}	0.81	0.78
1475.774	217,147	(e)	7/2	284,908	(o)	5/2	7.15×10^{9}	6.85×10^{9}	0.39	0.36
1478.758	202,173	(e)	11/2	269,797	(o)	9/2	4.89×10^{7} *	3.81×10^{9}	−1.77 *	0.10
1484.176	207,779	(e)	7/2	275,157	(o)	7/2	6.76×10^{9}	2.95×10^{9}	0.36	−0.01
1485.582	243,539	(e)	13/2	310,853	(o)	15/2	2.13×10^{10}	2.07×10^{10}	0.87	0.85
1487.908	220,182	(e)	5/2	287,390	(o)	7/2	5.69×10^{8}	2.65×10^{8}	−0.70	−1.04
1493.883	219,261	(e)	7/2	286,201	(o)	9/2	1.61×10^{8}	1.52×10^{8}	−1.25	−1.28
1499.728	201,310	(e)	11/2	267,988	(o)	11/2	6.00×10^{9}	9.72×10^{8}	0.31	−0.48
1500.734	207,779	(e)	7/2	274,413	(o)	5/2	6.23×10^{9}	5.47×10^{9}	0.33	0.27
1500.995	201,310	(e)	11/2	267,932	(o)	9/2	8.65×10^{9}	1.55×10^{9}	0.47	−0.28
1510.946	207,216	(e)	9/2	273,400	(o)	9/2	3.22×10^{8}	8.63×10^{8}	−0.95	−0.52
1516.850	218,982	(e)	5/2	284,908	(o)	5/2	2.62×10^{8}	1.72×10^{8}	−1.02	−1.20
1519.401	202,173	(e)	11/2	267,988	(o)	11/2	1.64×10^{8}	9.52×10^{8}	−1.23	−0.48
1520.695	202,173	(e)	11/2	267,932	(o)	9/2	2.13×10^{8}	1.49×10^{9}	−1.12	−0.29
1523.901	207,779	(e)	7/2	273,400	(o)	9/2	2.22×10^{9}	5.29×10^{8}	−0.11	−0.70
1536.335	220,182	(e)	5/2	285,271	(o)	7/2	2.30×10^{8}	5.68×10^{7}	−1.07	−1.67
1544.949	220,182	(e)	5/2	284,908	(o)	5/2	2.23×10^{8}	3.47×10^{8}	−1.07	−0.88
1584.538	212,047	(e)	9/2	275,157	(o)	7/2	3.00×10^{8}	1.32×10^{9}	−0.93	−0.31
1629.368	212,047	(e)	9/2	273,421	(o)	7/2	4.62×10^{8}	6.28×10^{8}	−0.73	−0.61
1647.007	207,216	(e)	9/2	267,932	(o)	9/2	2.44×10^{7}	2.06×10^{8}	−1.99	−1.06
1677.768	228,377	(e)	7/2	288,068	(o)	9/2	4.85×10^{7} *	4.61×10^{7}	−1.68 *	−1.76
1709.023	217,422	(e)	9/2	275,935	(o)	11/2	2.58×10^{7} *	5.81×10^{7}	−1.92 *	−1.59
1721.095	212,047	(e)	9/2	270,150	(o)	11/2	3.16×10^{9}	1.03×10^{9}	0.17	−0.33
1723.849	217,147	(e)	7/2	275,157	(o)	7/2	3.35×10^{7} *	7.94×10^{7}	−1.81 *	−1.45
1728.896	211,957	(e)	11/2	269,797	(o)	9/2	4.86×10^{9}	1.94×10^{9}	0.36	−0.05
1731.593	212,047	(e)	9/2	269,797	(o)	9/2	1.15×10^{9}	4.77×10^{8}	−0.27	−0.66
1736.574	218,982	(e)	5/2	276,567	(o)	7/2	1.75×10^{9}	9.55×10^{8}	−0.08	−0.35
1741.985	220,182	(e)	5/2	277,587	(o)	5/2	1.45×10^{9}	1.37×10^{9}	−0.17	−0.19

Table 1. *Cont.*

λ (Å) [a]	Lower Level [b]			Upper Level [b]			gA (s^{-1}) [c]		log gf [c]	
	E (cm^{-1})	(P)	J	E (cm^{-1})	(P)	J	HFR [d]	MCDHF [e]	HFR [d]	MCDHF [e]
1757.639	228,377	(e)	7/2	285,271	(o)	7/2	3.70×10^7 *	1.25×10^9	−1.76 *	−0.24
1760.697	200,497	(e)	13/2	257,293	(o)	13/2	3.79×10^9	3.50×10^9	0.25	0.21
1773.513	220,182	(e)	5/2	276,567	(o)	7/2	9.71×10^8	3.47×10^8	−0.32	−0.76
1775.340	243,552	(e)	11/2	299,879	(o)	11/2	1.23×10^9	1.06×10^9	−0.23	−0.30
1775.921	207,216	(e)	9/2	263,525	(o)	9/2	3.22×10^8	2.93×10^9	−0.81	0.15
1776.176	218,982	(e)	5/2	275,283	(o)	5/2	1.50×10^9	1.38×10^9	−0.15	−0.18
1777.040	217,147	(e)	7/2	273,421	(o)	7/2	1.32×10^9	1.16×10^9	−0.20	−0.26
1777.677	217,147	(e)	7/2	273,400	(o)	9/2	2.83×10^9	4.10×10^9	0.13	0.29
1780.161	218,982	(e)	5/2	275,157	(o)	7/2	2.21×10^8	1.13×10^9	−0.96	−0.25
1783.126	219,202	(e)	3/2	275,283	(o)	5/2	2.64×10^8	1.46×10^8 #	−0.90	−1.15 #
1783.513	200,497	(e)	13/2	256,566	(o)	11/2	8.14×10^9	7.86×10^9	0.59	0.58
1784.713	211,957	(e)	11/2	267,988	(o)	11/2	1.58×10^9	2.36×10^9	−0.12	0.06
1785.034	219,261	(e)	7/2	275,283	(o)	5/2	2.81×10^9	2.83×10^9	0.13	0.13
1785.199	228,377	(e)	7/2	284,393	(o)	9/2	3.13×10^9	4.04×10^9	0.18	0.29
1785.749	243,552	(e)	11/2	299,551	(o)	13/2	8.61×10^9	8.45×10^9	0.61	0.60
	217,422	(e)	9/2	273,421	(o)	7/2	4.48×10^9	4.18×10^9	0.33	0.30
1786.254	201,310	(e)	11/2	257,293	(o)	13/2	7.43×10^9	3.98×10^9	0.55	0.28
1786.411	217,422	(e)	9/2	273,400	(o)	9/2	1.91×10^9	2.45×10^9	−0.04	0.07
1786.501	211,957	(e)	11/2	267,932	(o)	9/2	1.81×10^9	4.46×10^9	−0.05	0.33
1787.584	212,047	(e)	9/2	267,988	(o)	11/2	3.44×10^9	5.29×10^9	0.22	0.41
1789.384	212,047	(e)	9/2	267,932	(o)	9/2	3.13×10^8	8.20×10^8	−0.81	−0.40
1789.056	219,261	(e)	7/2	275,157	(o)	7/2	1.66×10^8	9.00×10^8	−1.08	−0.35
1790.865	228,554	(e)	9/2	284,393	(o)	9/2	2.01×10^9	2.46×10^9	−0.01	0.08
1793.854	207,779	(e)	7/2	263,525	(o)	9/2	4.22×10^9	3.84×10^9	0.31	0.27
1800.399	207,779	(e)	7/2	263,323	(o)	7/2	1.59×10^9	1.52×10^9	−0.11	−0.13
1809.730	201,310	(e)	11/2	256,566	(o)	11/2	1.49×10^9	7.05×10^8	−0.13	−0.46
1811.205	219,202	(e)	3/2	274,413	(o)	5/2	5.02×10^8	6.33×10^8	−0.58	−0.48
1814.240	202,173	(e)	11/2	257,293	(o)	13/2	1.42×10^8	3.30×10^9	−1.14	0.21
1819.006	220,182	(e)	5/2	275,157	(o)	7/2	2.80×10^7	1.53×10^8	−1.83	−1.09
1838.460	202,173	(e)	11/2	256,566	(o)	11/2	3.49×10^7	6.11×10^8	−1.74	−0.51
1843.938	220,182	(e)	5/2	274,413	(o)	5/2	3.05×10^8	4.34×10^8	−0.78	−0.63

[a] Experimental wavelengths measured by Kaufman and Sugar [2] and Ryabtsev et al. [4]. [b] Lower and upper levels of the transitions are represented by their experimental values (in cm^{-1}), their parities ((e) for even and (o) for odd) and their J-values. Level energies (rounded values) are taken from Kaufman and Sugar [2] and Ryabtsev et al. [4]. [c] Weighted transition probabilities (gA) and oscillator strengths (log gf) computed in the present work (see text). [d] gA- and log gf-values with the * symbol correspond to transitions for which $CF < 0.05$ in the HFR calculations (see text). [e] gA- and log gf-values with the # symbol correspond to transitions for which $dT > 0.20$ in the MCDHF calculations (see text).

The HFR results listed in this table are those obtained using the Slater electrostatic parameters scaled down by a factor of 0.85 for the reasons described in Section 2.1. It was verified that most of the HFR transition rates given in Table 1 were not affected by cancelation effects. As a reminder, such an effect can be evaluated using the cancelation factor (CF) defined by the expression [5]:

$$CF = \left[\frac{\left| \sum\sum y^{\gamma}_{\beta J} \beta J P^{(1)} \beta' J' y^{\gamma'}_{\beta' J'} \right|}{\sum\sum \left| y^{\gamma}_{\beta J} \beta J P^{(1)} \beta' J' y^{\gamma'}_{\beta' J'} \right|} \right]^2 \quad (1)$$

where $P^{(1)}$ is the dipole operator for the transition between two atomic states $|\gamma J>$ and $|\gamma' J'>$ developed in terms of pure basis states $|\beta J>$ and $|\beta' J'>$, with $y^{\gamma}{}_{\beta J}$ and $y^{\gamma'}{}_{\beta'}{}_{J'}$ as mixing coefficients, respectively. According to Cowan [5], very small values (typically smaller than 0.05) of this quantity may be expected to show large percentage errors in the computed line strengths. In our work, it was found that the CF values were greater than 0.05 for the large majority of the lines listed in Table 1. This means that the corresponding line strengths were not altered by destructive interferences in our HFR calculations and can therefore be considered with confidence. The few transitions for which $CF < 0.05$ are indicated in the table. For these transitions, representing only 19% of the total number of the lines considered, the HFR transition probabilities and oscillator strengths should be taken with care.

Regarding the MCDHF gA- and log gf-values, the results listed in Table 1 are those obtained using the CV model in the Babushkin gauge, which corresponds to the length formalism in the non-relativistic limit. The accuracy of these radiative rates can be evaluated by the agreement with the data computed in the Coulomb gauge (velocity formalism) using the quantity dT defined by Ekman et al. [19] as:

$$dT = \frac{|A_B - A_C|}{\max(A_B, A_C)} \tag{2}$$

where A_B and A_C are transition probabilities in Babushkin and Coulomb gauges, since the electric dipole transition moment has the same value in both of these formalisms for exact solutions of the Dirac equation [20]. For approximate solutions, the transition moment differs so that the parameter dT provides a statistical estimate of the uncertainties on the MCDHF transition probabilities and oscillator strengths. For transitions listed in Table 1, we found that the average value of dT was equal to 0.1011 ± 0.1111, which means that the uncertainties affecting most of our MCDHF radiative rates do not exceed 20%. The few exceptions, i.e., transitions for which the dT value exceeds 20%, are marked in the table. They concern only 38 lines among a total of 457.

A reasonable overall agreement was found when comparing our HFR and MCDHF radiative rates for the whole set of transitions, the mean relative difference $\Delta A/\max(A_{\mathrm{HFR}}, A_{\mathrm{MCDHF}})$, where $\Delta A = A_{\mathrm{HFR}} - A_{\mathrm{MCDHF}}$, being found equal to -0.050 ± 0.498. As expected, the agreement between both methods was found to be better when excluding the transitions for which $CF < 0.05$ and $dT > 0.20$ in the HFR and MCDHF calculations, respectively. In this case, the mean relative deviation was reduced to -0.012 ± 0.424. These comparisons are illustrated in Figure 6 where the HFR log gf-values are plotted against the MCDHF ones. We note that a comparable general agreement was observed between HFR and MCDHF calculations recently performed in Lu IV [21]. For lower ionization stages of lutetium, larger discrepancies could be expected knowing that it is more complicated to obtain a convergence of the results, particularly with the MCDHF method, for neutral and weakly ionized atoms.

Finally, when comparing the data obtained in the present work with the gA-values calculated by Ryabtsev et al. [4] for the 23 experimentally observed lines they classified in their paper, we found an average agreement of 31% and 56% for our HFR and MCDHF results, respectively. It should be noted that for the same set of lines, the average agreement between HFR and MCDHF transition probabilities was found to be equal to 32%.

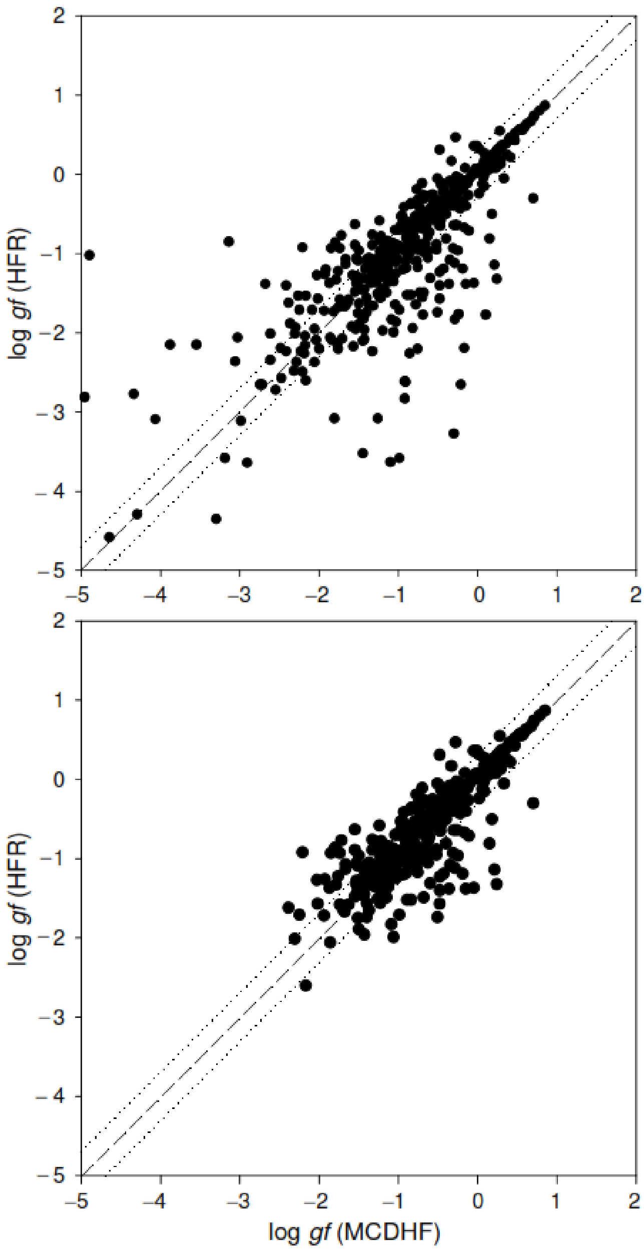

Figure 6. Comparison between the oscillator strengths (log *gf*) calculated in the present work using the HFR and the MCDHF methods for the experimentally identified spectral lines in Lu V. The top figure shows all the transitions and the bottom one includes only transitions for which *CF* > 0.05 and *dT* < 0.20 in the HFR and MCDHF calculations, respectively. The dashed line represents the strict equality and the dotted lines correspond to an agreement of a factor two between both sets of results.

4. Applications to Opacity Calculations for Kilonovae

In view of their production in large quantities during neutron star mergers, lanthanides give rise to numerous lines in the kilonovae spectra and therefore contribute largely to the opacities characterizing the latter. The atomic calculations performed in the present work were thus a good opportunity to estimate the opacity due to the Lu V ion in the context of early emission phases of kilonovae. To this end, we used the expansion opacity formalism developed by Sobelev [22], in which the absorption coefficient is given by:

$$\kappa(\lambda) = \frac{1}{ct\rho} \sum_l \frac{\lambda_l}{\Delta\lambda} \left(1 - e^{-\tau_l}\right) \tag{3}$$

where c (in cm s^{-1}) is the speed of light, t (in s) is the time after the merger, ρ (in g.cm^{-3}) is the density of the ejected gas, λ_l are the wavelengths of the lines appearing in the range $\Delta\lambda$ and τ_l are the corresponding optical depths expressed by the formula:

$$\tau_l = \frac{\pi e^2}{m_e c} f_l n_l t \lambda_l \tag{4}$$

where e (in C) is the elementary charge, m_e (in g) is the electron mass, f_l (dimensionless) is the oscillator strength and n_l (in cm^{-3}) is the density of the lower level of the transition.

Assuming the local thermodynamic equilibrium (LTE), n_l can be expressed by the Boltzmann distribution:

$$n_l = \frac{g_l}{U_z(T)} n e^{-E_l/k_B T} \tag{5}$$

where k_B is the Boltzmann constant (in cm^{-1} K^{-1}); T (in K) is the temperature, g_l and E_l (in cm^{-1}) are the statistical weight and the energy of the lower level of the transition, respectively; $U_z(T)$ is the partition function for the charge state z considered; and n is the corresponding ion density, which can be defined by the formula [23]:

$$n = \frac{\rho}{A m_p} f_z \tag{6}$$

where A is the mass number, m_p is the proton mass and f_z is the relative ionic fraction of the ionization degree z. In our case, we used the hypothesis where there was only Lu V (f_z = 1) in the plasma, which obliges us to choose the temperature corresponding to 100% of this charge state, according to the Saha equation. Since the resolution of the latter systematically led to the same temperature, i.e., T = 25,000 K, for the maximum abundance of other quadruply charged lanthanide ions such as La V, Ce V, Pr V, Nd V and Pm V in our previous works [10–12], this temperature was therefore also assumed in the present work for computing the opacity due to Lu V. Moreover, density $\rho = 10^{-10}$ g.cm^{-3} and time after merger t = 0.1 day were considered in the calculations, as suggested by Banerjee et al. [23] for early phases of kilonovae during which the V$^{\text{th}}$ spectra are expected to be produced.

The expansion opacity thus calculated for Lu V is shown in Figure 7. It is worth mentioning that this result was obtained using the radiative rates deduced from our HFR model for all the transitions below the ionization potential (IP = 538,700 cm^{-1} [1]) for which the oscillator strengths were found to be greater than 10^{-5}. This represents a total of 1,334,122 transitions. In addition, the wavelength width appearing in Equation (3) was chosen to be $\Delta\lambda$ = 10 Å. Looking at this figure, we see that the expansion opacity varies roughly between 4.5 and 0.001 cm^{2}g^{-1}, the maximum of opacity being located around 500 Å.

Interesting is the comparison we can make with the opacities we have already calculated under similar conditions for other quadruply ionized lanthanide atoms, namely La V, Ce V, Pr V, Nd V and Pm V [10–12]. Such a comparison is shown in Figure 8, in which the computed opacities obtained for these ions are plotted along with the one we estimated in the present work for Lu V. When looking at this figure, we clearly see that the maximum opacity appears at the same wavelength range in the spectrum, around 500 Å, for all the ions considered, with a preponderance of about one order of magnitude for Nd, Pm and Lu over La, Ce and Pr. On the other hand, beyond 500 Å, the contribution of Nd predominates on the whole spectrum.

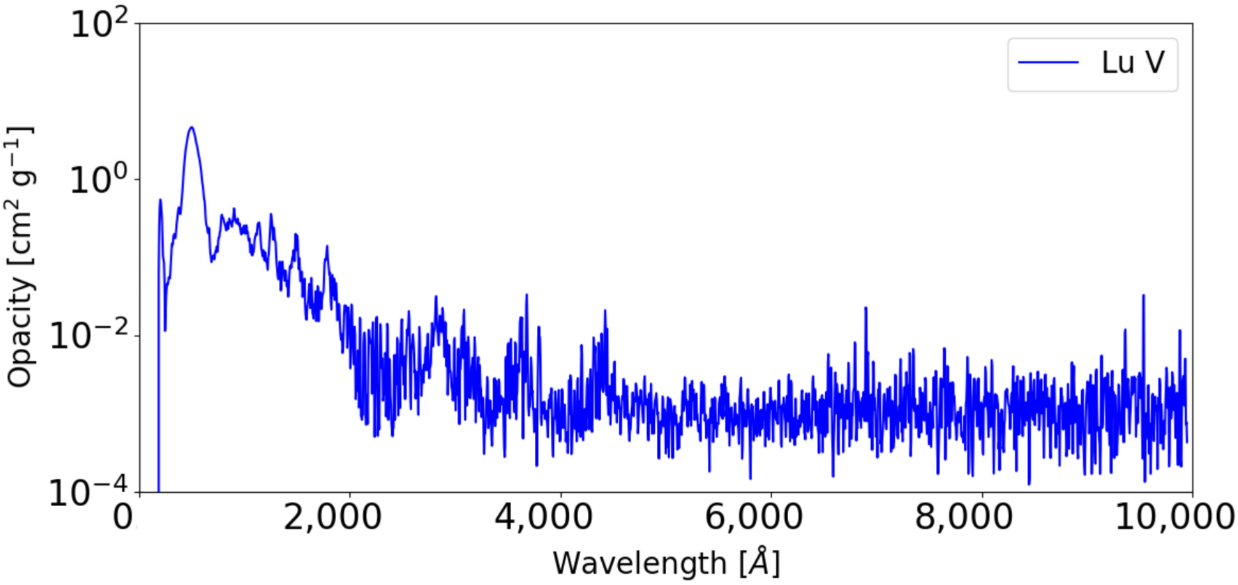

Figure 7. Expansion opacity for Lu V calculated with T = 25,000 K, $\rho = 10^{-10}$ g.cm^{-3}, t = 0.1 day and $\Delta\lambda$ = 10 Å.

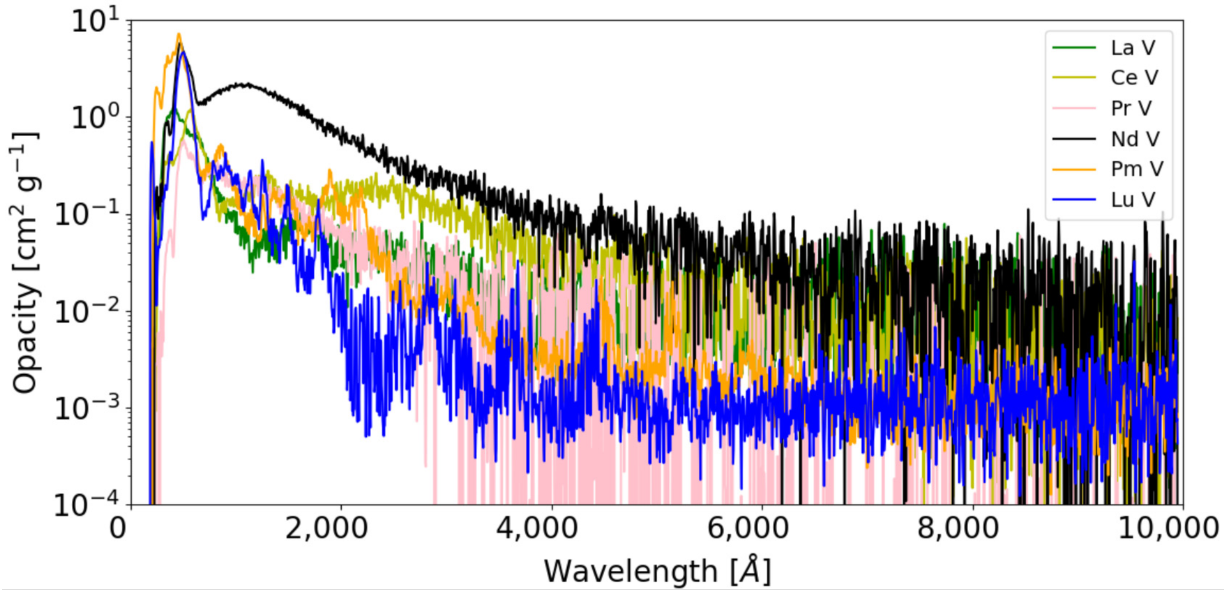

Figure 8. Comparison between the opacities obtained for quadruply charged La, Ce, Pr, Nd, Pm and Lu ions in the same kilonova conditions (T = 25,000 K, $\rho = 10^{-10}$ g.cm^{-3}, t = 0.1 day and $\Delta\lambda$ = 10 Å). The results for La V, Ce V, Pr V, Nd V and Pm V are taken from our previous calculations [10–12], while those for Lu V were deduced in the present work.

5. Conclusions

A consistent set of transition probabilities and oscillator strengths was obtained for a large amount of spectral lines in Lu V. The use of two independent theoretical approaches based on the HFR and MCDHF methods, as well as detailed comparisons with the few previously published data, allowed us to estimate the accuracy of the results deduced from our calculations. The new radiative rates were considered for determining the corresponding opacity in the case of kilonova conditions conducive to a maximum abundance of quadruply charged lanthanide ions (T = 25,000 K, $\rho = 10^{-10}$ g.cm^{-3}, t = 0.1 day). When comparing with our similar studies recently performed for La V, Ce V, Pr V, Nd V and Pm V ions, we also showed that, although the contribution of Lu V to the maximum opacity around 500 Å is as preponderant as that due to Nd V and Pm V ions, it is the Nd opacity which predominates on the whole spectrum.

Author Contributions: Conceptualization, H.C.G. and P.Q.; methodology, L.M., H.C.G. and P.Q.; software, H.C.G.; validation, L.M., H.C.G. and P.Q.; formal analysis, L.M.; investigation, L.M. and H.C.G.; resources, H.C.G. and P.Q.; data curation, L.M., H.C.G. and P.Q.; writing—original draft preparation, P.Q.; writing—review and editing, H.C.G. and P.Q.; visualization, P.Q.; supervision, P.Q.; project administration, H.C.G. and P.Q.; funding acquisition, P.Q. All authors have read and agreed to the published version of the manuscript.

Funding: This research was funded by F.R.S.-FNRS—EOS grant number O.0004.22.

Acknowledgments: H.C.G. is holder of a FRIA fellowship and P.Q. is Research Director of the Belgian Fund for Scientific Research F.R.S.-FNRS. This project received funding from the FWO and F.R.S.-FNRS under the Excellence of Science (EOS) programme (number O.0004.22). Part of the atomic calculations were made with computational resources provided by the Consortium des Equipements de Calcul Intensif (CECI), funded by the F.R.S.-FNRS under grant no. 2.5020.11 and by the Walloon Region of Belgium.

Conflicts of Interest: The authors declare no conflict of interest.

References

1. Kramida, A.; Ralchenko, Y.; Reader, J.; NIST ASD Team. *NIST Atomic Spectra Database*; National Institute of Standards and Technology: Gaithersburg, MD, USA, 2022. Available online: http://physics.nist.gov/asd (accessed on 28 August 2022).
2. Kaufman, V.; Sugar, J. Analysis of the spectrum of four-times-ionized lutetium (Lu V). *J. Opt. Soc. Am.* **1978**, *68*, 1529–1541. [CrossRef]
3. Racah, G. Theory of complex spectra II. *Phys. Rev.* **1942**, *62*, 438–462. [CrossRef]
4. Ryabtsev, A.; Kononov, E.; Kildiyarova, R.; Tchang-Brillet, W.-Ü.L.; Wyart, J.-F.; Champion, R.; Blaess, C. Spectra of W VIII and W IX in the EUV region. *Atoms* **2015**, *3*, 273. [CrossRef]
5. Cowan, R.D. *The Theory of Atomic Structure and Spectra*; University of California Press: Berkeley, CA, USA, 1981.
6. Kaufman, V.; Sugar, J. National Institute of Standards and Technology, Gaithersburg, MD, USA. 1980; Unpublished line list.
7. Abbott, B.P.; Abbott, R.; Abbott, T.D.; Acernese, F.; Ackley, K.; Adams, C.; Adams, T.; Addesso, P.; Adhikari, R.X.; Adya, V.B.; et al. GW170817: Observation of gravitational waves from a binary neutron star inspiral. *Phys. Rev. Lett.* **2017**, *119*, 161101. [CrossRef] [PubMed]
8. Abbott, B.P.; Abbott, R.; Abbott, T.D.; Acernese, F.; Ackley, K.; Adams, C.; Adams, T.; Addesso, P.; Adhikari, R.X.; Adya, V.B.; et al. Gravitational waves and gamma-rays from a binary neutron star merger: GW170817 and GRB 170817A. *Astrophys. J.* **2017**, *848*, L13. [CrossRef]
9. Kasen, D.; Metzger, B.; Barnes, J.; Quataert, E.; Ramirez-Ruiz, E. Origin of the heavy elements in binary neutron-star mergers from a gravitational-wave event. *Nature* **2017**, *551*, 80. [CrossRef] [PubMed]
10. Carvajal Gallego, H.; Berengut, J.C.; Palmeri, P.; Quinet, P. Atomic data and opacity calculations in La V-X ions for the investigation of kilonova emission spectra. *Mon. Not. R. Astron. Soc.* **2022**, *513*, 2302. [CrossRef]
11. Carvajal Gallego, H.; Berengut, J.C.; Palmeri, P.; Quinet, P. Large scale atomic data calculations in Ce V-X ions for application to early kilonova emission from neutron star mergers. *Mon. Not. R. Astron. Soc.* **2022**, *509*, 6138. [CrossRef]
12. Carvajal Gallego, H.; Deprince, J.; Berengut, J.; Palmeri, P.; Quinet, P. Opacity calculations in four to nine times ionized Pr, Nd and Pm atoms for the spectral analysis of kilonovae. *Mon. Not. R. Astron. Soc.* **2022**. submitted.
13. Quinet, P.; Palmeri, P.; Biémont, E. On the use of Cowan's code for atomic structure calculations in singly ionized lanthanides. *J. Quant. Spectrosc. Radiat. Transf.* **1999**, *62*, 625. [CrossRef]
14. Quinet, P.; Palmeri, P.; Biémont, E.; McCurdy, M.M.; Rieger, G.; Pinnington, E.H.; Wickliffe, M.E.; Lawler, J.E. Experimental and theoretical lifetimes, branching fractions and oscillator strengths in Lu II. *Mon. Not. R. Astron. Soc.* **1999**, *307*, 934. [CrossRef]
15. Quinet, P.; Palmeri, P.; Biémont, E.; Li, Z.S.; Zhang, Z.G.; Svanberg, S. Radiative lifetime measurements and transition probability calculations in lanthanide ions. *J. Alloys Compd.* **2002**, *344*, 255. [CrossRef]
16. Grant, I.P. *Relativistic Quantum Theory of Atoms and Molecules*; Springer: New York, NY, USA, 2007.
17. Froese Fischer, C.; Godefroid, M.R.; Brage, T.; Jönsson, P.; Gaigalas, G. Advanced multiconfiguration methods for complex atoms: I. Energies and wave functions. *J. Phys. B At. Mol. Opt. Phys.* **2016**, *49*, 182004. [CrossRef]
18. Froese Fischer, C.; Gaigalas, G.; Jönsson, P. GRASP2018—A Fortran 95 version of the General Relativistic Atomic Structure Package. *Comput. Phys. Commun.* **2019**, *237*, 184. [CrossRef]
19. Ekman, J.; Godefroid, M.R.; Hartman, H. Validation and implementation of uncertainty estimates of calculated transition Rates. *Atoms* **2014**, *2*, 215. [CrossRef]
20. Grant, I.P. Gauge invariance and relativistic radiative transitions. *J. Phys. B* **1974**, *7*, 1458. [CrossRef]

21. Bokamba Motoumba, E.; Enzonga Yoca, S.; Quinet, P.; Palmeri, P. Calculations of transition rates in erbium-like ions Lu IV, Hf V and Ta VI using the ab initio MCDHF-RCI and semi-empirical HFR methods. *At. Data Nucl. Data Table* **2020**, *133–134*, 101340. [CrossRef]
22. Sobolev, V.V. *Moving Envelopes of Stars*; Harvard University Press: Cambridge, UK, 1960.
23. Banerjee, S.; Tanaka, M.; Kawaguchi, K.; Kato, D.; Gaigalas, G. Simulations of early kilonova emission from neutron star mergers. *Astrophys. J. Suppl. Ser.* **2020**, *901*, 29. [CrossRef]